nature metabolism

Letter

https://doi.org/10.1038/s42255-023-00931-7

Glucose-dependent insulinotropic polypeptide regulates body weight and food intake via GABAergic neurons in mice

Received: 15 July 2023

Accepted: 13 October 2023

Published online: 9 November 2023

Check for updates

Arkadiusz Liskiewicz[1,2,3], Ahmed Khalil[1,2], Daniela Liskiewicz[1,2,4], Aaron Novikoff[1,2], Gerald Grandl[1,2], Gandhari Maity-Kumar[1,2], Robert M. Gutgesell[1,2], Mostafa Bakhti[2,5], Aimée Bastidas-Ponce[2,5], Oliver Czarnecki[2,5,6], Konstantinos Makris[1,2], Heiko Lickert[2,5,6], Annette Feuchtinger[7], Monica Tost[7], Callum Coupland[1,2], Lisa Ständer[1,2], Seun Akindehin[1,2], Sneha Prakash[1,2], Faiyaz Abrar[1,2], Russell L. Castelino[1,2], Yantao He[8], Patrick J. Knerr[8], Bin Yang[8], Wouter F. J. Hogendorf[8], Shiqi Zhang[5], Susanna M. Hofmann[5,9], Brian Finan[8], Richard D. DiMarchi[10], Matthias H. Tschöp[11,12], Jonathan D. Douros[8] & Timo D. Müller[1,2] ✉

The development of single-molecule co-agonists for the glucagon-like peptide-1 (GLP-1) receptor (GLP-1R) and glucose-dependent insulinotropic polypeptide (GIP) receptor (GIPR) is considered a breakthrough in the treatment of obesity and type 2 diabetes. But although GIPR–GLP-1R co-agonism decreases body weight with superior efficacy relative to GLP-1R agonism alone in preclinical[1–3] and clinical studies[4,5], the role of GIP in regulating energy metabolism remains enigmatic. Increasing evidence suggests that long-acting GIPR agonists act in the brain to decrease body weight through the inhibition of food intake[3,6–8]; however, the mechanisms and neuronal populations through which GIP affects metabolism remain to be identified. Here, we report that long-acting GIPR agonists and GIPR–GLP-1R co-agonists decrease body weight and food intake via inhibitory GABAergic neurons. We show that acyl-GIP decreases body weight and food intake in male diet-induced obese wild-type mice, but not in mice with deletion of *Gipr* in *Vgat* (also known as *Slc32a1*)-expressing GABAergic neurons (*Vgat-Gipr* knockout). Whereas the GIPR–GLP-1R co-agonist MAR709 leads, in male diet-induced obese wild-type mice, to greater weight loss and further inhibition of food intake relative to a pharmacokinetically matched acyl-GLP-1 control, this superiority over GLP-1 vanishes in *Vgat-Gipr* knockout mice. Our data demonstrate that long-acting GIPR agonists crucially depend on GIPR signaling in inhibitory GABAergic neurons to decrease body weight and food intake.

The development of GIPR–GLP-1R co-agonists have been a major advancement in the treatment of obesity and diabetes[9], but the mechanisms through which GIP affects systemic energy metabolism remain largely unknown. Accumulating evidence indicates that long-acting GIPR agonists act in the brain to decrease body weight through inhibition of food intake[3,6–8]. Chemogenetic activation of hypothalamic and hindbrain GIPR neurons decreases food intake in mice[6,7] and long-acting GIPR agonists decrease body weight and food intake in obese wild-type

A full list of affiliations appears at the end of the paper. e-mail: timodirk.mueller@helmholtz-munich.de

mice[3,8], but not in mice with *Nes-cre*-mediated neuronal loss of *Gipr*[3]. Accumulating evidence indicates that GIPR agonism is also a vital constituent to GIPR–GLP-1R co-agonism. The GIPR–GLP-1R co-agonist MAR709 leads relative to a pharmacokinetically matched acyl-GLP-1 to greater weight loss and further inhibition of food intake, but this superiority vanishes in mice with neuronal loss of *Gipr*[3]. And while the GIPR–GLP-1R co-agonist tirzepatide promotes insulin secretion in isolated human islets primarily via the GIP receptor[10], long-acting GIPR agonists attenuate the emetic effect of GLP-1R agonism in experimental animals[11,12] and hence likely contribute to greater tolerability of GIPR–GLP-1R co-agonism relative to GLP-1R agonism at higher doses. Although the mechanisms and neuronal populations through which GIP affects body weight and food intake have yet to be identified, these data collectively indicate that GIPR agonism is a vital constituent to the metabolic efficacy and tolerability of GIPR–GLP-1R co-agonism.

Several studies have recently assessed the expression profile of *Gipr* in the brain using single-cell RNA-sequencing (scRNA-seq) analysis, revealing that *Gipr* is expressed in a variety of different cells types within the hypothalamus and the hindbrain, including neurons, mesenchymal cells, mural cells and oligodendrocytes[7,13–15]. In both of these brain areas, expression of *Gipr* is found in cells or neurons that express *Slc32a1* (also known as *Vgat*), a marker indicative of inhibitory GABAergic neurons[6,14,16,17]. GABAergic *Gipr* neurons seem crucial for the anti-emetic effect of GIPR agonism[11,13], but their role in energy metabolism remains unknown. Emphasizing their potential role in energy balance regulation, *Vgat*-expressing GABA neurons are implicated in the control of eating behavior[18–20], and while optogenetic stimulation of VGAT neurons in the lateral hypothalamus promotes food intake, genetic ablation of these neurons has the opposite effect[18]. Although being expressed in only 14–18% of all *Gipr* cells in the hypothalamus[15] and the hindbrain[14], *Vgat* it is found in around 32% of hypothalamic *Gipr* neurons[15] and, depending on the study, in up to 55% of hindbrain *Gipr* neurons[14,16,17,21] (Extended Data Table 1). Based on the expression of *Gipr* in GABAergic neurons[7,11,14,15], and the demonstration that selective activation of hypothalamic and hindbrain GIPR neurons decreases food intake in mice[6,7], we here assessed whether the metabolic effects of GIP and GIPR–GLP-1R co-agonism depend on GIPR signaling in inhibitory GABAergic neurons.

High-fat diet (HFD)-fed male *Vgat-Gipr* knockout (KO) mice show decreased body weight and improved glucose metabolism. Mice with deletion of *Gipr* in inhibitory GABAergic neurons were generated by crossing C57BL/6J $Gipr^{flx/flx}$ mice[22,23] with C57BL/6J *Vgat-ires-cre* knock-in mice (Jackson Laboratories; 028862), which express Cre recombinase under control of the *Vgat* promoter. Consistent with scRNA-seq data showing that *Vgat* is only expressed in 14–18% of all *Gipr*-expressing cells in the hypothalamus[15] and hindbrain[14] (Extended Data Table 1), *Vgat-cre*$^{+/-}$*Gipr*$^{flx/flx}$ mice (*Vgat-Gipr* KO) show relative to *Vgat-cre*$^{+/-}$*Gipr*$^{wt/wt}$ controls (wild-type) no overt changes in *Gipr* expression in either the hypothalamus or the hindbrain (Extended Data Fig. 1a,b). *Vgat-Gipr* KO mice show further no decreased expression of *Gipr* in the pancreas, isolated pancreatic islets, epididymal white adipose tissue (eWAT), peripheral nervous system (sciatic nerve, dorsal root ganglia and trigeminal ganglion) and the gut (duodenum, jejunum, ileum and colon) (Extended Data Fig. 1c–l). But consistent with the phenotype seen in mice with *Nes-cre*-mediated neuronal loss of *Gipr*[3], male *Vgat-Gipr* KO mice show, relative to wild-type controls, decreased body weight when chronically fed HFD (Fig. 1a). The decreased body weight in *Vgat-Gipr* KO mice is accompanied by decreased fat and lean tissue mass (Fig. 1b,c) and is mediated by decreased food intake (Fig. 1d) without alterations in nutrient absorption (Fig. 1e,f), substrate utilization (Fig. 1g) or fatty acid oxidation (Fig. 1h). Male *Vgat-Gipr* KO mice show no difference in energy expenditure, although locomotor activity is increased (Fig. 1i,j). Similar to mice with global[24] or neuronal[3] loss of *Gipr*, HFD-fed male *Vgat-Gipr* KO mice exhibit decreased fasting levels of blood glucose and insulin (Fig. 1k,l), improved insulin sensitivity (Fig. 1m,n) and improved glucose control that is, however, lost after normalizing to baseline glucose levels (Fig. 1o,p). Male *Vgat-Gipr* KO mice show no differences in pancreatic islet size, α- and β-cell mass and insulin and glucagon immunoreactivity (Extended Data Fig. 1m–s). No differences are observed in glycated hemoglobin (HbA1c) or plasma levels of triglycerides, cholesterol and free fatty acids (Fig. 1q–t). Also, ad libitum levels of plasma $GLP\text{-}1_{total}$ and GIP_{total} are unchanged between *Vgat-Gipr* KO mice and wild-type controls (Extended Data Fig. 1a,b). But consistent with the lower body fat mass (Fig. 1b), HFD-fed male *Vgat-Gipr* KO mice show decreased plasma levels of leptin, reduced hepatosteatosis and reduced adipocyte size in the inguinal white adipose tissue (Extended Data Fig. 2c–f). No differences are observed in hypothalamic expression of proopiomelanocortin (*Pomc*), cocaine and amphetamine-regulated transcript (*Cart*), neuropeptide y (*Npy*), agouti-related peptide (*Agrp*), somatostatin (*Sst*), arginine vasopressin (*Avp*), tachykinin precursor 1 (*Tac1*), parathyroid hormone-like hormone (*Pthlh*), amyloid-β precursor like protein 1 (*Aplp1*) or cystatin c (*Cst3*) (Extended Data Fig. 2g–p), or in hindbrain expression of cholecystokinin (*Cck*), GLP-1R (*Glp1r*), hypocretin neuropeptide precursor (*Hcrt*) or oxytocin (*Oxt)* (Extended Data Fig. 2q–t). Collectively, male *Vgat-Gipr* KO mice largely resemble the phenotype of *Nes-Gipr* KO mice[3] as reflected by decreased body weight and food intake, and improved glucose control when fed a HFD.

We found that chow-fed male *Vgat-Gipr* KO mice show normal body weight but improved glucose metabolism. Male *Vgat-Gipr* KO mice also mimic the phenotype of the global[24] and neuronal[3] *Gipr* KO mice when fed a regular chow diet. Chow-fed *Vgat-Gipr* KO mice show no overt differences in body weight, body composition or food intake relative to wild-type controls (Fig. 2a–d). Absorption and utilization of nutrients is also not different between chow-fed *Vgat-Gipr* KO mice and wild-type controls (Fig. 2e–g), although fatty acid oxidation is decreased in the *Vgat-Gipr* KO mice (Fig. 2h). *Vgat-Gipr* KO mice show no differences in locomotor activity (Fig. 2i), energy expenditure (Fig. 2j) or fasting levels of blood glucose (Fig. 2k), but insulin levels are decreased (Fig. 2l). Chow-fed *Vgat-Gipr* KO mice further show improved glucose tolerance (Fig. 2m) without alterations in insulin sensitivity (Fig. 2n) or plasma levels of triglycerides and cholesterol (Fig. 2o,p). Similar to the chow-fed male *Vgat-Gipr* KO mice, female *Vgat-Gipr* KO mice show no difference in body weight relative to wild-type controls, even when fed a HFD (Extended Data Fig. 3a). Female *Vgat-Gipr* KO mice show no difference in body composition or food intake relative to wild-type controls, but locomotor activity is slightly enhanced, without changes in fatty acid oxidation, nutrient utilization and energy expenditure (Extended Data Fig. 3b–h). Female *Vgat-Gipr* KO mice further show decreased blood glucose with normal fasting levels of plasma insulin, but improved glucose tolerance without changes in insulin sensitivity, HbA1c and plasma levels of triglycerides, cholesterol and free fatty acids (Extended Data Fig. 3i–p).

We found that *Vgat-Gipr* KO mice are resistant to central GIP effects on cFos neuronal activation and food intake. Based on recent data indicating that GIP acts on hindbrain GIPR neurons to regulate food intake[6], we next assessed whether validated long-acting (fatty acid acylated) GLP-1R and GIPR agonists[2,3,8] (Extended Data Fig. 4a) differ in their ability to induce neuronal activation in this area. After single subcutaneous administration, we find fluorescently labeled acyl-$GLP\text{-}1^{Cy5}$ and acyl-GIP^{Cy5} to substantially accumulate in the area postrema (Fig. 3a); however, although we find acyl-$GLP\text{-}1^{Cy5}$ to induce cFos neuronal activity in the area postrema and the nucleus tractus solitarius (NTS), acyl-GIP^{Cy5} induced cFos activity only in the area postrema, but not in the NTS (Fig. 3a–c). Notably, while acyl-GIP^{Cy5} in wild-type mice solidly induced cFos activity in the area postrema, this effect was largely blunted in the *Vgat-Gipr* KO mice, despite unchanged accumulation of acyl-GIP^{Cy5} in the area postrema (Fig. 3d,e). Preserved accumulation of acyl-GIP^{Cy5} in the area postrema of the *Vgat-Gipr* KO mice is not unexpected, given that *Vgat* is only expressed in ~18% of *Gipr* cells in

https://doi.org/10.1038/s42255-023-00931-7

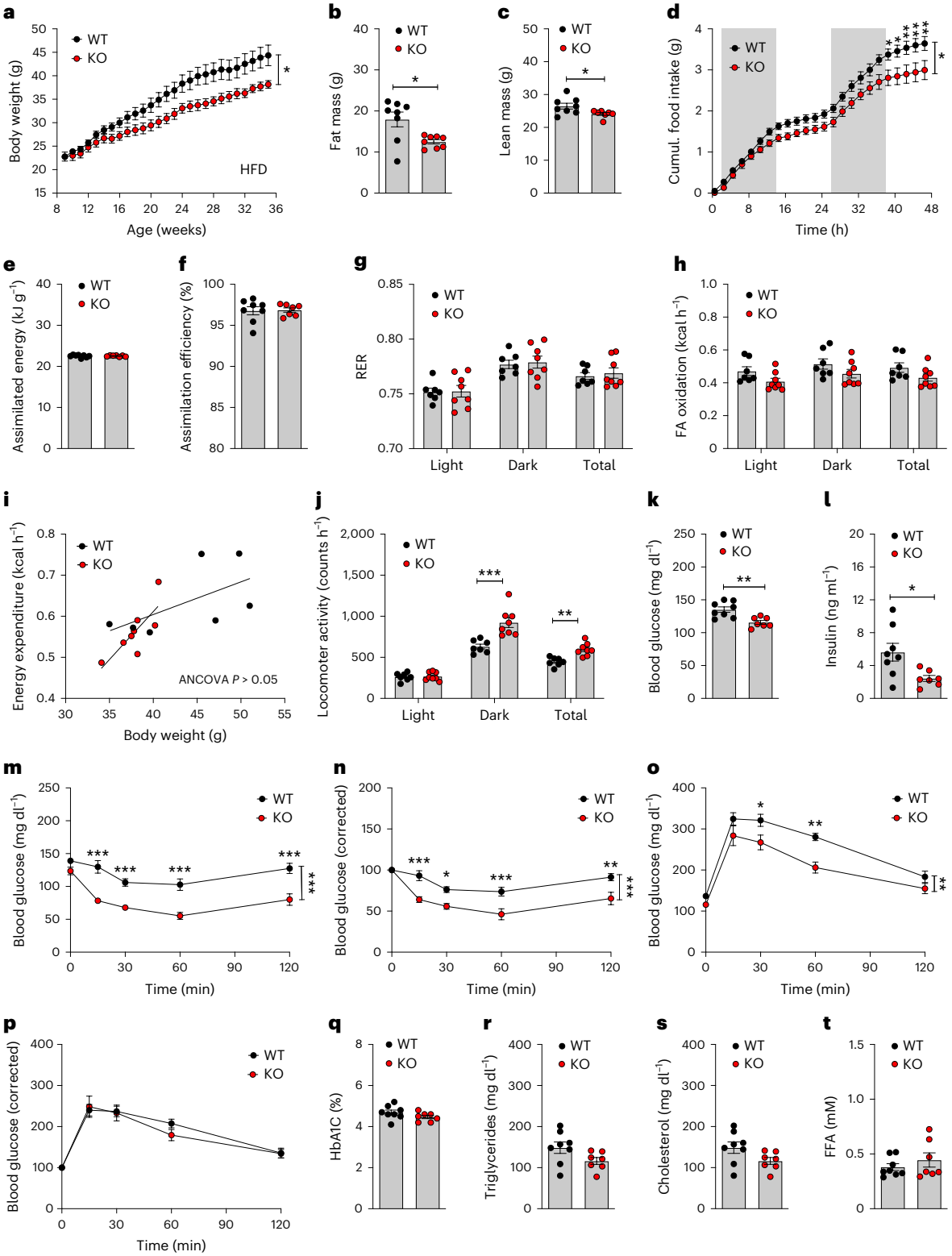

Fig. 1 | Metabolic characterization of HFD-fed *Vgat-Gipr* KO mice. a–**c**, Body weight development (**a**) and body composition of 35-week-old male C57BL/6J wild-type (WT) and *Vgat-Gipr* knockout (KO) mice ($n = 7$–8 each group) (**b**,**c**). **d**–**f**, Food intake in 35-week-old male C57BL/6J mice ($n = 7$ each group) (**d**) as well as assimilated energy and assimilation efficiency in 35-week-old male C57BL/6J mice ($n = 7$–8 each group) (**e**,**f**). **g**–**j**, Respiratory exchange ratio (RER) (**g**), fatty acid (FA) oxidation (**h**), energy expenditure (**i**) and locomotor activity (**j**) in 35-week-old male C57BL/6J mice ($n = 7$–8 each group). **k**,**l**, Fasting levels of blood glucose (**k**) and insulin (**l**) in 37-week-old male C57BL/6J mice ($n = 7$–8 each group). **m**–**p**, Intraperitoneal insulin tolerance in 38-week-old male C57BL/6J mice ($n = 7$–8 each group) (**m**,**n**) and glucose tolerance in 34-week-old male C57BL/6J mice (**o**,**p**). **q**–**t**, HbA1c (**q**) and plasma levels of triglycerides (**r**), cholesterol (**s**) and free fatty acids (FFA) (**t**) in 40-week-old male C57BL/6J mice ($n = 7$–8 each group). Data in **a**,**d**,**m**–**p** were analyzed by repeated measures two-way analysis of variance (ANOVA) with Bonferroni's post hoc test for comparison of individual time points. Data in **b**,**c**,**e**–**h**,**j**,**k**,**l**,**q**–**t** were analyzed using a Student's two-sided, two-tailed *t*-test. Data in **i** were analyzed using ANCOVA with body weight as covariate. Date are mean ± s.e.m.; $^{*}P < 0.05$; $^{**}P < 0.01$ and $^{***}P < 0.001$. Individual *P* values are shown in the Source Data file, unless $P < 0.0001$.

https://doi.org/10.1038/s42255-023-00931-7

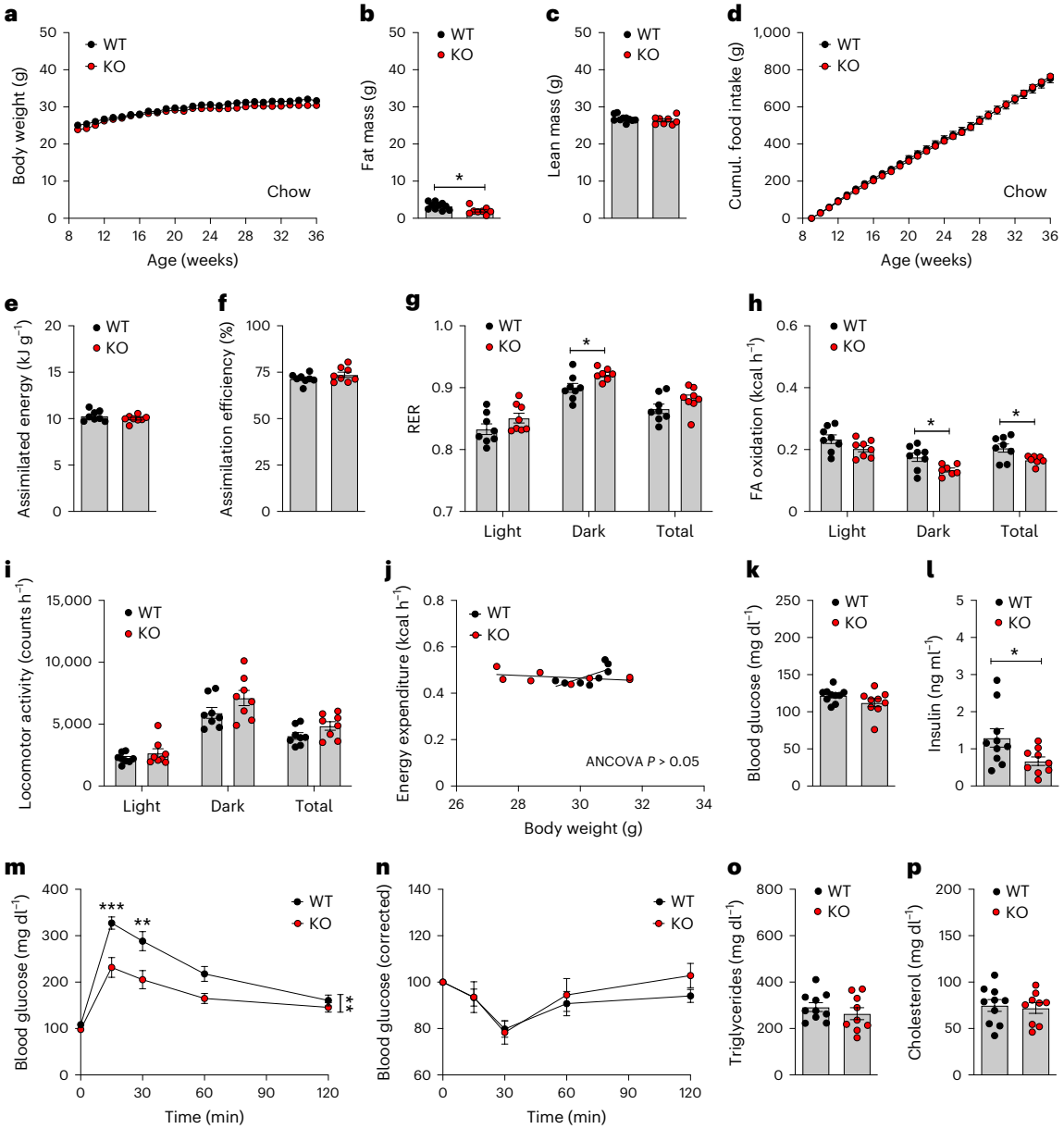

Fig. 2 | Metabolic characterization of chow-fed *Vgat-Gipr* KO mice. a–c, Body weight development ($n = 9–10$ each group) (**a**) and body composition ($n = 8–10$ each group) of 36-week-old male C57BL/6J WT and *Vgat-Gipr* KO mice (**b**,**c**). **d–f**, Food intake in 36-week-old male C57BL/6J mice ($n = 8–10$ each group) (**d**) as well as assimilated energy and assimilation efficiency in 36-week-old male C57BL/6J mice ($n = 8$ each group) (**e**,**f**). **g–j**, RER (**g**), fatty acid oxidation (**h**), locomotor activity (**i**) and energy expenditure (**j**) in 36-week-old male C57BL/6J mice ($n = 8$ each group). **k**,**l**, Fasting levels of blood glucose (**k**) and insulin (**l**) in 38-week-old male C57BL/6J mice ($n = 9–10$ each group). **m**,**n**, Glucose tolerance in 38-week-old male C57BL/6J mice ($n = 9–10$ each group) (**m**) and insulin tolerance (**n**) in 39-week-old male C57BL/6J mice ($n = 8–10$ each group). **o**,**p**, Ad libitum plasma levels of triglycerides (**o**) and cholesterol (**p**) in 40-week-old male C57BL/6J mice ($n = 9–10$ each group). Data in **a**,**d**,**m**,**n** were analyzed by repeated measures two-way ANOVA with Bonferroni's post hoc test for comparison of individual time points. Data in **b**,**c**,**e–i**,**k**,**l**,**o**,**p** were analyzed using a Student's two-tailed *t*-test. Data in **j** were analyzed using ANCOVA with body weight as covariate. Cumulative food intake in **d** was assessed per cage in $n = 8–10$ double-housed mice. Date are mean ± s.e.m.; $^{*}P < 0.05$; $^{**}P < 0.01$ and $^{***}P < 0.001$. Individual *P* values are shown in the Source Data file, unless $P < 0.0001$.

the hindbrain, including for example oligodendrocytes and endothelial cells[14] (Extended Data Table 1). Nonetheless, consistent with previous scRNA-seq data showing that *Vgat* is particularly enriched in *Gipr* neurons within the area postrema[11,13–15,17,21] (Extended Data Table 1), these data hence demonstrate that the acyl-GIP^{Cy5}-induced cFos activation in the area postrema is almost exclusively attributed to *Vgat*-expressing inhibitory GABAergic neurons. In wild-type and *Vgat-Gipr* KO mice, we also found that acyl-GIP^{Cy5}, after a single subcutaneous administration, accumulates in the hypothalamic median eminence, along with increased cFos activation in the arcuate nucleus and paraventricular nucleus in wild-type mice, but not in *Vgat-Gipr* KO mice (Extended Data Fig. 5a–d). No changes were observed in cFos activation in the ventromedial and dorsomedial hypothalamus (Extended Data Fig. 5b,e,f) or the lateral parabrachial nucleus (Extended Data Fig. 5gh). We next assessed whether acyl-GIP differentially affects food intake in HFD-fed diet-induced obese (DIO) wild-type and *Vgat-Gipr* KO mice. While single subcutaneous bolus administration of acyl-GIP (100 nmol kg^{-1}) acutely decreased food intake in male and female HFD-fed wild-type mice, administration of acyl-GIP failed to affect food intake in male and female *Vgat-Gipr* KO mice (Fig. 3f–i). These data hence indicate

https://doi.org/10.1038/s42255-023-00931-7

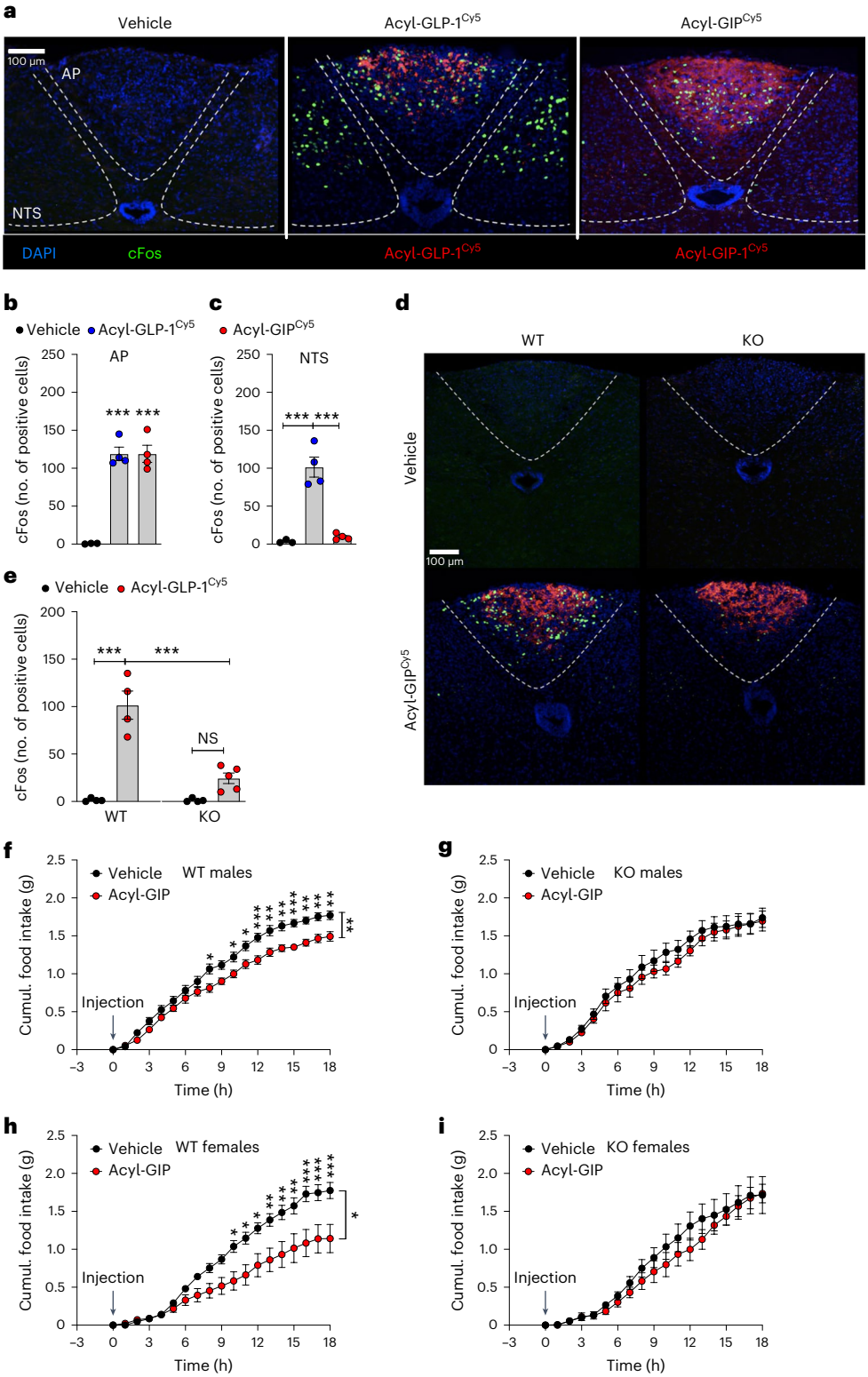

Fig. 3 | Acyl-GIP effects on cFos neuronal activation in the hindbrain and acute food intake in HFD-fed *Vgat-Gipr* KO mice. a–**c**, Representative image (**a**) and quantification (**b**,**c**) of cFos-positive neurons, as well as fluorescently (Cy5)-labeled drug appearance, in the area postrema (AP) and NTS of 52-week-old C57BL/6J WT mice treated with a single subcutaneous bolus (150 nmol kg^{-1}) of either acyl-GLP-1^{Cy5} or acyl-GIP^{Cy5} (n = 3–4 mice each group). DAPI, 4,6-diamidino-2-phenylindole. **d**,**e**, Representative image (**d**) and quantification (**e**) of cFos-positive neurons, as well as Cy5-labeled drug appearance, in the area postrema of 26-week-old male C57BL/6J WT and *Vgat-Gipr* KO mice treated with a single subcutaneous dose of either vehicle or acyl-GIPCy5 (150 nmol kg^{-1}; n = 4–5 each group) (**d**). **f**,**g**, Cumulative food intake in 35-week-old male C57BL/6J WT (**f**) and *Vgat-Gipr* KO (**g**) mice treated with a single subcutaneous dose of either vehicle or acyl-GIP (100 nmol kg^{-1}, n = 7 each group). **h**,**i**, Cumulative food intake in 40-week-old female C57BL/6J WT (**h**) and *Vgat-Gipr* KO (**i**) mice treated with a single subcutaneous dose of either vehicle or acyl-GIP (100 nmol kg^{-1}, n = 6–10 each group). Data in **b**,**c**,**e** were analyzed using an ordinary one-way ANOVA. Data in **f**–**i** were analyzed using repeated measures two-way ANOVA and a Bonferroni multiple comparison test for individual time points. Scale bars, 100 µm. Data are mean ± s.e.m.; NS, not significant; *P < 0.05; **P < 0.01 and ***P < 0.001. Individual P values are shown in the Source Data file, unless P < 0.0001.

https://doi.org/10.1038/s42255-023-00931-7

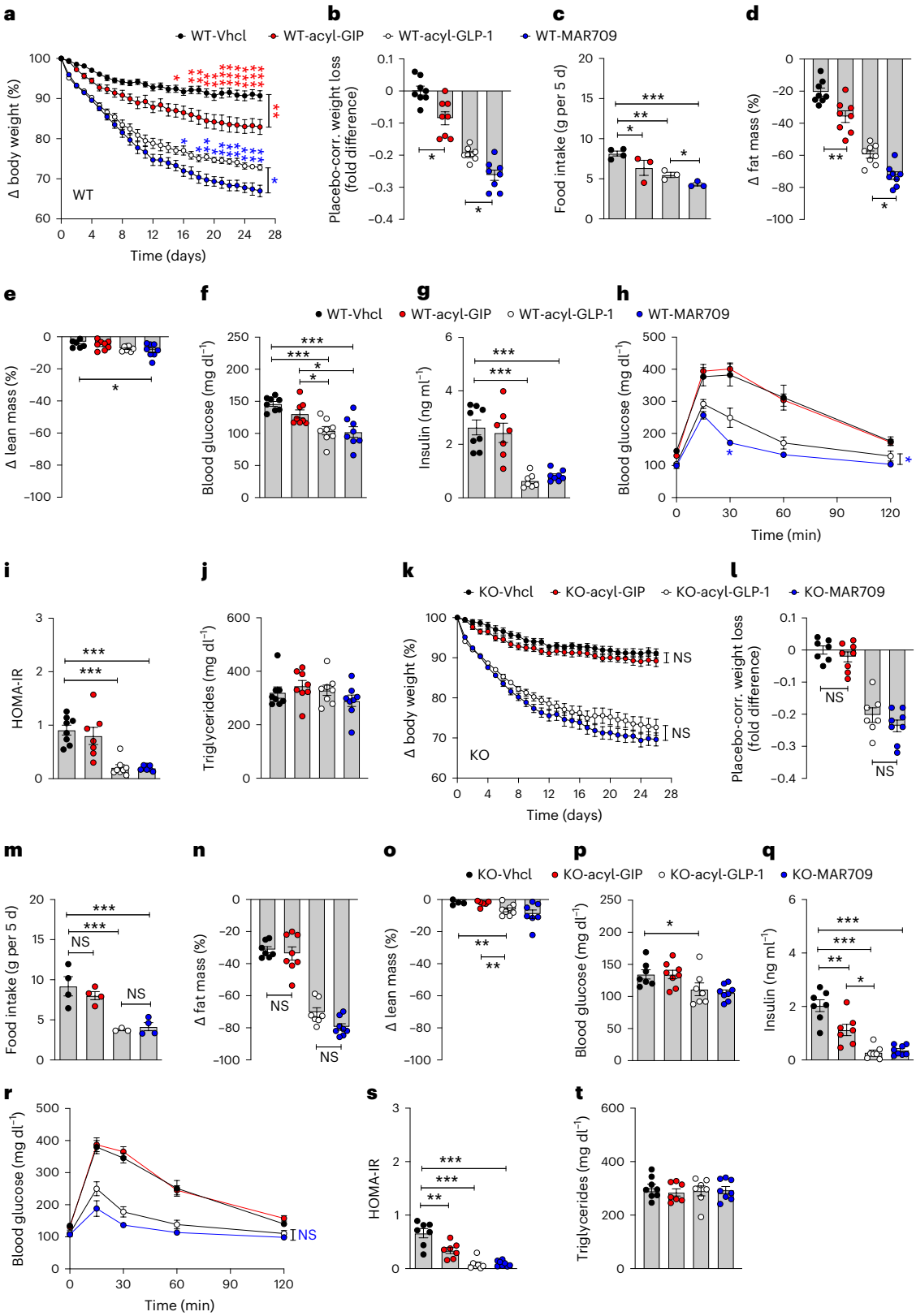

that acyl-GIP essentially requires GIPR signaling in *Vgat*-expressing inhibitory GABAergic neurons to acutely decrease food intake.

We found that GIP and GIPR–GLP-1R co-agonism decreases body weight and food intake in mice via GIPR signaling in inhibitory GABAergic neurons. We assessed whether the body weight-lowering effect of acyl-GIP and GIPR–GLP-1R co-agonism depend on GIPR signaling in GABAergic neurons. In DIO wild-type mice, daily subcutaneous treatment with acyl-GIP (100 nmol kg^{-1}) for 26 days significantly decreased body weight and food intake relative to vehicle controls (Fig. 4a–c and Extended Data Fig. 6a,b). The decrease in body weight in mice treated with acyl-GIP was accompanied by a decrease in fat but not lean tissue mass (Fig. 4d,e), without overt changes in blood glucose, insulin,

https://doi.org/10.1038/s42255-023-00931-7

Fig. 4 | Effects of acyl-GIP, acyl-GLP-1 and MAR709 on body weight and glucose metabolism in HFD-fed *Vgat-Gipr* KO mice. a–c, Body weight development (**a**), placebo-corrected weight loss after 26 days of treatment (**b**), and food intake (**c**) of 38-week-old male C57BL/6J WT mice treated daily with vehicle (Vhcl), acyl-GIP (100 nmol kg^{-1}) or 10 nmol kg^{-1} of either acyl-GLP-1 or MAR709 ($n = 7–8$ each group). **d–j**, Fat and lean tissue mass in 38-week-old male C57BL/6J WT mice (**d**,**e**), fasting levels of blood glucose and insulin in 38-week-old male C57BL/6J WT mice (**f**,**g**), glucose tolerance in 38-week-old male C57BL/6J WT mice (**h**), HOMA-IR in 38-week-old male WT mice (**i**) and plasma levels of triglycerides in 35-week-old male C57BL/6J WT mice (**j**) ($n = 7–8$ each group). **k–m**, Body weight development (**k**), placebo-corrected weight loss after 26 days of treatment (**l**) and food intake (**m**) of 35-week-old male C57BL/6J *Vgat-Gipr* KO mice treated daily with vehicle, acyl-GIP (100 nmol kg^{-1}) or 10 nmol kg^{-1} of either acyl-GLP-1 or MAR709 ($n = 7–8$ each group). **n–t**, Fat and lean tissue mass in 35-week-old male C57BL/6J KO mice (**n**,**o**), fasting levels of blood glucose and insulin in 35-week-old male WT mice (**p**,**q**), glucose tolerance in 35-week-old male C57BL/6J WT mice (**r**), HOMA-IR in 35-week-old male WT mice (**s**) and plasma levels of triglycerides in 35-week-old male C57BL/6J WT mice (**t**) ($n = 7–8$ mice each group). Data in **a**,**h**,**k**,**r** were analyzed using repeated measures two-way ANOVA and with Bonferroni post hoc comparison for individual time points. Data in **c**,**m** were analyzed using Fishers LSD test. Data in **b**,**d–g**,**i**,**j**,**l**,**n–q**,**s**,**t** were analyzed using ordinary one-way ANOVA. Data in **g**,**i** were analyzed using a Student's two-tailed *t*-test. Food intake in **c**,**m** was assessed per cage in double-housed mice. Cages with mice shredding food were excluded from the analysis. Data area mean ± s.e.m.; NS, not significant; $^{*}P < 0.05$; $^{**}P < 0.01$ and $^{***}P < 0.001$. Individual *P* values are shown in the Source Data file, unless $P < 0.0001$.

glucose tolerance, insulin sensitivity or plasma levels of triglycerides (Fig. 4f–j). Consistent with the ability of acyl-GIP to decrease body weight and food intake in DIO wild-type mice (Fig. 4a–c), treatment with the GIPR–GLP-1R co-agonist MAR709 led to greater weight loss and further decrease in food intake and fat mass relative to mice treated with acyl-GLP-1 (Fig. 4a–d). In DIO wild-type mice, MAR709 and acyl-GLP-1 equally decreased fasting levels of blood glucose and insulin (Fig. 4f–g), but with superiority of MAR709 over acyl-GLP-1 to improve glucose tolerance (Fig. 4h). Insulin sensitivity, as estimated by HOMA-IR, was equally improved by MAR709 and acyl-GLP-1 (Fig. 4i), without effects of either treatment on plasma levels of triglycerides (Fig. 4j).

In contrast to DIO wild-type mice, treatment with acyl-GIP in *Vgat-Gipr* KO mice failed to affect body weight, food intake or body composition relative to vehicle controls (Fig. 4k–o). Treatment of *Vgat-Gipr* KO mice with acyl-GIP had no effect on blood glucose despite a slight decrease in fasting insulin levels (Fig. 4p,q). *Vgat-Gipr* KO mice treated with acyl-GIP show no difference in glucose control relative to vehicle controls, but display improved insulin sensitivity, as estimated by HOMA-IR (Fig. 4r,s), without changes in plasma triglycerides (Fig. 4t). Consistent with the demonstration that acyl-GIP loses its ability to decrease body weight and food intake in *Vgat-Gipr* KO mice (Fig. 4k–m), we found that weight loss induced by MAR709 was indistinguishable from that under acyl-GLP-1 treatment in *Vgat-Gipr* KO mice (Fig. 4k,l). The observed superiority of MAR709 over acyl-GLP-1 to further inhibit food intake in wild-type mice (Fig. 4c) likewise vanished in the *Vgat-Gipr* KO mice (Fig. 4m). MAR709 and acyl-GLP-1 further equally decreased fat mass, as well as fasting levels of blood glucose and insulin in *Vgat-Gipr* KO mice (Fig. 4o–q), with nearly identical improvements in glucose tolerance and insulin sensitivity (Fig. 4e,s) and unchanged plasma levels of triglycerides (Fig. 4t). In summary, these data show that GIPR signaling in inhibitory GABAergic neurons is essential for the ability of acyl-GIP to decrease body weight and food intake and also, for the superior metabolic effects of the GIPR–GLP-1R co-agonist MAR709 over a matched acyl-GLP-1 control. Our data are consistent with our previous report demonstrating that acyl-GIP and MAR709 act in the brain to regulate body weight and food intake via central nervous system GIPR signaling[3]. Furthermore, our data corroborate that GIPR signaling is a genuine contributor to the metabolic efficacy of GIPR–GLP-1R co-agonism, in that it drives greater weight loss and further inhibition of food intake relative to GLP-1R agonism alone. Notably, our data are further in line with the recent demonstration that a long-acting GIPR agonist decreases body weight in healthy humans[25].

We here show that long-acting GIPR agonists and the GIPR–GLP-1R co-agonist MAR709 decrease body weight and food intake in DIO mice via GIPR signaling in inhibitory GABAergic neurons. Limitations to our study include the lack of publicly available antibodies to reliably detect GIPR, which would be of value to further delineate the neuronal mechanisms by which GIP regulates energy metabolism in GABAergic neurons. Such antibodies would have also been useful to demonstrate lack of co-staining between VGAT and GIPR in *Vgat-Gipr* KO mice and to further characterize the *Vgat*/*Gipr* coexpressing neurons. Published scRNA repositories[14,16,17,21], however, show that ~81–93% of the *Vgat*/*Gipr*-expressing cells in the hypothalamus and the dorsal vagal complex (DVC) are neurons (Extended Data Fig. 6c) and that *Vgat*/*Gipr* coexpressing neurons in the DVC belong to five out of seven GABAergic neuron clusters with ~37% and ~19% localizing to clusters GABA5 and GABA4, respectively (Extended Data Fig. 6d–g).

Further limitations of our studies include that we cannot exclude the potential for variable long-acting GIPR agonists to differ in central GIPR signaling based on differences in pharmacokinetics and pharmacodynamics. Differences in pharmacokinetics might also explain why we see that acyl-GIP^{Cy5} restricted cFos activation in the area postrema, whereas other studies using different GIPR agonists found cFos activation in the NTS[6,11]. Although unlikely, the possibility that the pharmacokinetics of the acyl-GIP that we used slightly differs from acyl-GIP^{Cy5} may be a similar consideration. Another limitation is that the HFD-fed wild-type and *Vgat-Gipr* KO mice had a strong tendency to shred food, which prevented deeper analysis of eating behavior, including assessment of cumulative food intake and meal patterns. Notably, the demonstrated low (~14–18%) abundance of *Vgat* in *Gipr* cells using scRNA-seq analysis may be an underestimate due to limitations in complementary DNA library preparations or due to the general difficulty to adequately detect low-abundant transcripts. Finally, clarification is needed on whether acyl-GIP and GIPR–GLP-1R co-agonists decrease body weight and food intake exclusively via hindbrain GABAergic neurons or whether also GABAergic GIPR neurons in other brain regions are required for the effects on body weight and food intake shown in this study.

Methods

Animals and housing conditions

Experiments were performed in accordance with the Animal Protection Law of the European Union after permission by the Government of Upper Bavaria. Mice were fed ad libitum with either chow diet (1314, Altromin) or HFD (D12331, Research Diets) and were kept at 22 ± 2 °C with constant humidity (45–65%) and a 12-h light–dark cycle. C57BL/6J *Vgat-ires-cre* knock-in mice were purchased from The Jackson Laboratory (028862). $Gipr^{flx/flx}$ mice[22,23] were crossed with $Vgat\text{-}cre^{+/-}$ mice to obtain $Vgat\text{-}cre^{+/-}$ $Gipr^{flx+/flx+}$ (*Vgat-Gipr* KO). $Vgat\text{-}cre^{+/-}Gipr^{flx-/flx-}$ were used as WT controls. For metabolic phenotyping and assessment of drug effects, age-matched mice were grouped based on genotype and double-housed at room temperature (22 ± 2 °C). For the examination of drug effects, mice were fed a HFD approximately 20 weeks before the start of the studies. Body composition was analyzed using a magnetic resonance whole-body composition analyzer (EchoMRI). For pharmacological studies, mice were treated for the indicated time duration with either acyl-GIP (100 nmol kg^{-1}) or 10 nmol kg^{-1} of acyl-GLP-1 or MAR709 (Extended Data Fig. 1a).

Drug development

Commercially available maleimide-functionalized fluorophores were conjugated to the free cysteine residue of the appropriate

peptide. For Cy5-labeled compounds, the peptide was dissolved to 3–5 mM in dimethylsulfoxide containing 0.5–2.5 equivalent EDTA and 1–2.5 equivalent of reductant (Tris(2-carboxyethyl)phosphine or bis(p-sulfonatophenyl)phenylphosphine). The pH was adjusted above pH 7 with eg 1% *v*/*v* DIPEA or 0.25 M phosphate, pH 7.4, followed by the addition of 1.3 equivalent of solid sulfo-cyanine3 maleimide, overnight stirring at room temperature and purification by reversed-phase HPLC. For Cy5-labeled compounds, the peptide was dissolved to 1–2 mM in PBS, pH 7.4, containing ~3 equivalent tris(2-carboxyethyl)phosphine. The pH was adjusted above pH 7 with 1 M NaOH, followed by the addition of 3 equivalent solid sulfo-cyanine5 maleimide, stirring for 30 min at room temperature and purification by reversed-phase HPLC.

Fasting glucose, insulin, ipGTT and ipITT

Fasting levels of blood glucose and insulin were measured in 6-h fasted mice. Insulin was measured by Ultra-Sensitive Mouse Insulin ELISA kit (90080, Crystal Chem) according to the manufacturer's instructions. For assessment of glucose tolerance, glucose was administered intraperitoneally at a dose of 1.75 g kg^{-1}. For assessment of insulin tolerance, insulin (Humalog, Eli Lilly and Co.) was injected intraperitoneally at a dose of 0.75 UI kg^{-1} (HFD-fed mice) or 0.5 UI kg^{-1} (chow-fed mice).

Bomb calorimetry

Assimilated energy and assimilation efficiency were assessed using the C200 Oxygen Bomb Calorimeter (IKA). Feces were collected over 7 days, dried at 65 °C until weight was consistent, before measuring the food/fecal energy content.

Indirect calorimetry

Energy expenditure, food intake, RER, FA oxidation and locomotor activity were assessed for 3–4 consecutive days in single-house mice using a climate-controlled indirect calorimetric system (TSE Phenomaster, TSE Systems). Mice were given a 24-h acclimatization phase before the start of the measurements. Data for energy expenditure were analyzed using ANCOVA with body weight as a covariate as previously suggested[26,27]. FA oxidation (kcal h^{-1}) was calculated by the formula, energy expenditure (kcal h^{-1}) × (1 − RER)/0.3 (ref. 28).

RNA extraction and gene expression analysis

For qPCR analysis, RNA was isolated using the RNeasy kit (74106, QIAGEN) according to the manufacturer's instructions. cDNA was synthesized using the QuantiTect RT kit (205311, QIAGEN) according to the manufacturer's instructions. Quantitative PCR was performed in two or three technical replicates per sample, using SYBR green (4309155, Thermo Fisher Scientific) using the Applied Biosystems QuantStudio 6 or 7 (Thermo Fisher Scientific). The following primers were used: *Pomc:* 5′-CATTAGGCTTGGAGCAGGTC-3′ and 5′-TCTTGATGATGGCGTTCTTG-3′; *Cartpt:* 5′-CGAGAAGA AGTACGGCCAAG-3′ and 5′-GGAATATGGGAACCGAAGGT-3′; *Npy:* 5′-TGGACTGACCCTCGCTCTAT-3′and5′-TGTCTCAGGGCTGGATCTCT-3′; *Agrp:* 5′-GGCCTCAAGAAGACAACTGC-3′ and 5′-GCAAAAGG CATTGAAGAAGC-3′); *Gipr* 5′-GTGTCCACGAGGTGGTGTTT-3′ and 5′-CCGACTGCACCTCTTTGTTG-3′; *Hprt:* 5′-AAGCTTGC TGGTGAAAAGGA-3′ and 5′-TTGCGCTCATCTTAGGCTTT-3′; *Ppia:* 5′-GAGCTGTTTGCAGACAAAGTTC-3′ and 5′-CCCTGGC ACATGAATCCTGG-3′; *Sst*: 5′-GAGCCCAACCAGACAGAGAA-3′ and 5′-CCTCATCTCGTCCTGCTCA-3′;*Avp:*5′-ACTACGCTCTCCGCTTGTTT-3′ and 5′-CAGCAGATGCTTGGTCCGAA-3′; *Tac1:* 5′-CGCACC TGCGGAGCAT-3′ and 5′-CTCAAAGGGCTCCGGCATT-3′; *Pthlh*: 5′-AGA AGCGAAGGACTCGGTCT-3′ and 5′-CCTGTAACGTGTCCTTGGAAGA-3′; *Aplp1*: 5′-CTTCAGGTGATCGAAGAGCGA-3′ and 5′-GGAGGCTA CCTTTGTCCTCA-3′; *Cst3:* 5′-CGCCATACAGGTGGTGAGAG-3′ and 5′-GGCTGGTCATGGAAAGGACA-3′; *Cck*: 5′-ACTGCTAGC GCGATACATCC-3′ and 5′-CATCCAGCCCATGTAGTCCC-3′; *Hcrt*: 5′-TCCTGCCGTCTCTACGAACT-3′ and 5′-TGGTTACCGT TGGCCTGAAG-3′; *Oxt:* 5′-CTGTGCTGGACCTGGATATGCG-3′ and 5′-AGCTCGTCCGCGCAGCAGATG-3′; *Glp1r*: 5′-AGCACT GTCCGTCTTCATCA-3′ and 5′-AGAAGGCCAGCAGTGTGTAT-3′; *Actb*: 5′-TTGCTGACAGGATGCAGAAG-3′ and 5′-ACATCTG CTGGAAGGTGGAC-3′. Target gene expression was assessed using the $\Delta\Delta C_t$ method[29]. The expression level of each gene was normalized to the housekeeping genes *Hprt, Ppia*, *Gapdh*, *Actb* or *Tbp*, depending on which genes showed the lowest variability across genotypes in the respective tissue.

Immunofluorescence

For assessment of cFos, mice were habituated to a daily injection by subcutaneous saline administration for three constitutive days. On day 4, mice were treated subcutaneous with a single dose of acyl-GIP^{Cy5} or acyl-GLP-1^{Cy5} (150 nmol kg^{-1}). The mice were exposed to CO_2 overdose 90 min after drug exposure and were briefly perfused with ice-cold TBS following by buffered 4% formaldehyde. Twenty-four hours after fixation, brains were coronally cryosectioned and 35-µm-thick slices were immunolabelled with the monoclonal rabbit anti-cFos antibody (MA5-15055, Invitrogen, 1:400 dilution) and the anti-rabbit Alexa546 secondary antibody (A10040, Invitrogen, 1:2,000 dilution). According to the Allen Mouse Brain Atlas, the DVC containing the area postrema and NTS was captured by ×20 objective in *z*-stack mode using a Leica SP8 confocal microscope. In each region, the number of cFos-positive cells was automatically counted in using Fiji/ImageJ software. For cFos quantification, whole brain slices were scanned in z-stack mode with AxioScan 7 digital slide scanner (Zeiss, ZEN Blue v.3.5, ×20 objective) and imaged using LAS X (v.3.5.7.23225, Leica Microsystems). The Allen Brain Atlas was imputed and aligned to the whole slide images using Fiji with the ABBA plugin and the number of cFos-positive cells in each identified region was measured by using QuPath v.0.4.4 software[30].

Immunohistochemistry for α- and β-cell volume and islet size

Pancreata were fixed in 10% formalin (HT501128, Sigma-Aldrich) for 24 h at room temperature and processed for paraffin embedding (Tissue Tec VIP.6, Sakura Europe). Paraffinized pancreata were exhaustively cross-sectioned into 3–4 parallel, equidistant slices per case. Maintaining their orientation, the tissue slices were vertically embedded in paraffin. After co-staining for insulin (monoclonal rabbit anti-insulin, 3014, Cell Signaling 1:800 dilution; AlexaFluor750-conjugated goat anti-rabbit, A21039, Invitrogen 1:100 dilution) and for glucagon (polyclonal guinea pig anti-glucagon, M182, Takara 1:3,000 dilution; goat anti-guinea pig AF555, A21435, Invitrogen 1:200 dilution) nuclei were labeled with Hoechst33342 (H1399, Thermo Fisher, 7.5 µg ml^{-1}). The stained tissue sections were scanned with an AxioScan 7 digital slide scanner (Zeiss, ZEN Blue v.3.5) equipped with a ×20 magnification objective. Quantification of insulin- or glucagon-expressing cells was performed on the entire tissue sections using the image analysis software Visiopharm. The insulin- or glucagon-expressing cells were classified automatically using the fluorescence intensity of each hormone. The β-cell volume (mg) was calculated by multiplying the detected relative insulin-positive cell area by total pancreatic weight. The α-cell volume (mg) was similarly calculated based on the detected glucagon-positive cell area. The area of the pancreatic islet was calculated based on the insulin and glucagon-positive area.

Islet isolation

Islets were isolated via collagenase P perfusion of the pancreas[31]. In brief, collagenase P solution (1 mg ml^{-1}, Roche) was injected through the ampulla of Vater and pancreata were digested at 37.5 °C for 12 min. Digestion was stopped by addition of ice-cold HBSS (Thermo Fisher), including 0.05% (*w*/*v*) BSA (Sigma-Aldrich). The tissue suspension was centrifuged and islets were purified by density gradient purification using 15% OptiPrep density gradient medium (Sigma-Aldrich). Islets in

the visible density gradient layer were collected, rinsed with HBSS and incubated in complete RPMI-1640 medium (Gibco) at 37 °C with 5 % CO_2.

Single-cell RNA-seq analysis

The published RNA-seq datasets[14–17,21] were analyzed using Scanpy (v.2.11.0)[32], Seurat v.5 (ref. 33) or CELLxGENE (v.1.1.2) (Chan Zuckerberg Initiative). The authors' original pre-processing and cell-type annotations were adopted without any changes. Only cells with at least one unique molecular identifier were considered in the analysis.

Serum analysis

Blood was collected by cardiac puncture during organ withdrawal, stored on ice and centrifuged (2,500*g* for 10 min at 4 °C) for serum separation and collection. The levels of leptin (KMC2281, Leptin mouse ELISA, Invitrogen), GIP (EZRMGIP-55K, rat/mouse GIP ELISA, Merck Millipore) and GLP-1 (1508, Mouse GLP-1 ELISA, Crystal Chem) were measured according to the manufacturer's instructions.

Histological analysis

Excised samples were fixed in 4% (w/v) neutrally buffered formalin, embedded in paraffin and cut into 3-µm slices for hematoxylin and eosin and scanned with an AxioScan 7 digital slide scanner (Zeiss) equipped with a ×20 magnification objective. Steatosis was graded by the presence of fat vacuoles in liver cells according to the percentage of affected tissue (0, <5%; 1, 5–33%; 2, 33–66%; and 3, >66%). Lobular inflammation was scored by overall assessment of inflammatory foci per ×200 field (0, no foci; 1, <2 foci; 2, 2–4 foci; and 3, >4 foci). The morphometric quantification of mean size of adipocytes was performed using the commercially available image analysis software Visiopharm (v. 2018.9; Visiopharm).

Statistical analysis

Statistical analyses were performed using GraphPad Prism v.9 and SPSS v.28.0.1.1. Analysis of energy expenditure were performed using ANCOVA with body weight as a covariate as previously suggested[26,27]. For each analysis, the statistical tests and sample sizes are indicated in the figure legends. $P < 0.05$ was considered statistically significant. All data represent mean ± s.e.m.

Reporting summary

Further information on research design is available in the Nature Portfolio Reporting Summary linked to this article.

Data availability

The data used for the statistical analysis are available in source data files, along with the GraphPad Prism-derived statistical reports as appropriate, which contain the mean difference between the treatment groups, 95% confidence intervals, the significance summary and exact *P* values (unless $P < 0.0001$). The used scRNA-seq datasets are available via the Gene Expression Omnibus under accession codes GSE160938, GSE166649 and GSE168737. The HypoMap is available in an interactive CELLxGENE viewer (https://www.mrl.ims.cam.ac.uk). The corresponding Seurat object is deposited at University of Cambridge's Apollo Repository (https://doi.org/10.17863/CAM.87955). Other used databases include the Allen Mouse Atlas. All raw images are provided in the source data files, with the exception of the histology pictures for Extended Data Figs. 1m–s and 2d–f, which were too large for public repositories; due to the large file size of these pictures, they are only available upon request. Source data are provided with this paper.

References

1. Coskun, T. et al. LY3298176, a novel dual GIP and GLP-1 receptor agonist for the treatment of type 2 diabetes mellitus: From discovery to clinical proof of concept. *Mol. Metab.* **18**, 3–14 (2018).
2. Finan, B. et al. Unimolecular dual incretins maximize metabolic benefits in rodents, monkeys, and humans. *Sci. Transl. Med.* **5**, 209ra151 (2013).
3. Zhang, Q. et al. The glucose-dependent insulinotropic polypeptide (GIP) regulates body weight and food intake via CNS-GIPR signaling. *Cell Metab.* **33**, 833–844 (2021).
4. Heise, T. et al. Effects of subcutaneous tirzepatide versus placebo or semaglutide on pancreatic islet function and insulin sensitivity in adults with type 2 diabetes: a multicentre, randomised, double-blind, parallel-arm, phase 1 clinical trial. *Lancet Diabetes Endocrinol.* **10**, 418–429 (2022).
5. Frias, J. P. et al. Tirzepatide versus semaglutide once weekly in patients with type 2 diabetes. *N. Engl. J. Med.* **385**, 503–515 (2021).
6. Adriaenssens, A. et al. Hypothalamic and brainstem glucose-dependent insulinotropic polypeptide receptor neurons employ distinct mechanisms to affect feeding. *JCI Insight* https://doi.org/10.1172/jci.insight.164921 (2023).
7. Adriaenssens, A. E. et al. Glucose-dependent insulinotropic polypeptide receptor-expressing cells in the hypothalamus regulate food intake. *Cell Metab.* **30**, 987–996 (2019).
8. Mroz, P. A. et al. Optimized GIP analogs promote body weight lowering in mice through GIPR agonism not antagonism. *Mol. Metab.* **20**, 51–62 (2019).
9. Muller, T. D., Bluher, M., Tschop, M. H. & DiMarchi, R. D. Anti-obesity drug discovery: advances and challenges. *Nat. Rev. Drug Discov.* **21**, 201–223 (2022).
10. El, K. et al. The incretin co-agonist tirzepatide requires GIPR for hormone secretion from human islets. *Nat. Metab.* **5**, 945–954 (2023).
11. Borner, T. et al. GIP receptor agonism attenuates GLP-1 receptor agonist-induced nausea and emesis in preclinical models. *Diabetes* **70**, 2545–2553 (2021).
12. Zhang, C., Vincelette, L. K., Reimann, F. & Liberles, S. D. A brainstem circuit for nausea suppression. *Cell Rep.* **39**, 110953 (2022).
13. Borner, T. et al. GIP receptor agonism blocks chemotherapy-induced nausea and vomiting. *Mol. Metab.* **73**, 101743 (2023).
14. Dowsett, G. K. C. et al. A survey of the mouse hindbrain in the fed and fasted states using single-nucleus RNA sequencing. *Mol. Metab.* **53**, 101240 (2021).
15. Steuernagel, L. et al. HypoMap-a unified single-cell gene expression atlas of the murine hypothalamus. *Nat. Metab.* **4**, 1402–1419 (2022).
16. Ludwig, M. Q., Todorov, P. V., Egerod, K. L., Olson, D. P. & Pers, T. H. Single-cell mapping of GLP-1 and GIP receptor expression in the dorsal vagal complex. *Diabetes* **70**, 1945–1955 (2021).
17. Ludwig, M. Q. et al. A genetic map of the mouse dorsal vagal complex and its role in obesity. *Nat. Metab.* **3**, 530–545 (2021).
18. Jennings, J. H. et al. Visualizing hypothalamic network dynamics for appetitive and consummatory behaviors. *Cell* **160**, 516–527 (2015).
19. Marino, R. A. M. et al. Control of food approach and eating by a GABAergic projection from lateral hypothalamus to dorsal pons. *Proc. Natl Acad. Sci. USA* **117**, 8611–8615 (2020).
20. Russo, F. M., De Bie, F. R., Partridge, E. A., Allegaert, K. & Deprest, J. The antenatal sildenafil STRIDER trial for severe fetal growth restriction, are post hoc reflections ad rem? *Eur. J. Pediatr.* **181**, 3775–3776 (2022).
21. Zhang, C. et al. Area postrema cell types that mediate nausea-associated behaviors. *Neuron* **109**, 461–472 (2021).
22. Campbell, J. E. et al. TCF1 links GIPR signaling to the control of β cell function and survival. *Nat. Med* **22**, 84–90 (2016).
23. Ussher, J. R. et al. Inactivation of the glucose-dependent insulinotropic polypeptide receptor improves outcomes following experimental myocardial infarction. *Cell Metab.* **27**, 450–460 e456 (2018).

24. Miyawaki, K. et al. Inhibition of gastric inhibitory polypeptide signaling prevents obesity. *Nat. Med* **8**, 738–742 (2002).
25. Knop, F. K. et al. A long-acting glucose dependent insulinotropic polypeptide receptor agonist shows weight loss without nausea or vomiting. In *American Diabetes Association – 83rd Annual Scientific Sessions;* San Diego, CA, USA; 23–26 June 2023 Poster 56-OR (ADA, 2023).
26. Muller, T. D., Klingenspor, M. & Tschop, M. H. Revisiting energy expenditure: how to correct mouse metabolic rate for body mass. *Nat. Metab.* **3**, 1134–1136 (2021).
27. Tschop, M. H. et al. A guide to analysis of mouse energy metabolism. *Nat. Methods* **9**, 57–63 (2011).
28. Liskiewicz, D. et al. Neuronal loss of TRPM8 leads to obesity and glucose intolerance in male mice. *Mol. Metab.* **72**, 101714 (2023).
29. Livak, K. J. & Schmittgen, T. D. Analysis of relative gene expression data using real-time quantitative PCR and the $2^{-\Delta\Delta CT}$ method. *Methods* **25**, 402–408 (2001).
30. Bankhead, P. et al. QuPath: open source software for digital pathology image analysis. *Sci. Rep.* **7**, 16878 (2017).
31. Li, D. S., Yuan, Y. H., Tu, H. J., Liang, Q. L. & Dai, L. J. A protocol for islet isolation from mouse pancreas. *Nat. Protoc.* **4**, 1649–1652 (2009).
32. Wolf, F. A., Angerer, P. & Theis, F. J. SCANPY: large-scale single-cell gene expression data analysis. *Genome Biol.* **19**, 15 (2018).
33. Satija, R., Farrell, J. A., Gennert, D., Schier, A. F. & Regev, A. Spatial reconstruction of single-cell gene expression data. *Nat. Biotechnol.* **33**, 495–502 (2015).

Acknowledgements

T.D.M. received funding for this work from the European Research Council ERC-CoG Trusted no. 101044445. T.D.M. also received funding from the German Research Foundation (TRR296, TRR152, SFB1123 and GRK 2816/1) and the German Center for Diabetes Research. M.H.T. received funding from the European Research Council AdG HypoFlam no. 695054. S.M.H. received funding from the German Research Foundation, SFB1123.

Author contributions

A.L., A.K., A.N., D.L., A.N., G.G., A.B.-P., G.M.-K., M.B., O.C., C.C., L.S., S.A., S.P., F.A. and R.L.C. performed experiments and analyzed and interpreted data. A.F., M.T., R.M.G., K.M. and S.Z. analyzed data. Y.H., P.J.K., B.Y. and W.F.J.H. developed drugs. B.F. and J.D.D. supervised drug development and participated in study design and data interpretation. R.D.D.M., M.H.T., S.M.H. and H.L. participated in data interpretation and edited the manuscript. T.D.M. conceptualized the project, supervised experiments, analyzed and interpreted data and wrote the manuscript together with A.L.

FundingInformation

Open access funding provided by Helmholtz Zentrum München - Deutsches Forschungszentrum für Gesundheit und Umwelt (GmbH).

Competing interests

M.H.T. is a member of the scientific advisory board of ERX Pharmaceuticals. He was a member of the Research Cluster Advisory Panel (ReCAP) of the Novo Nordisk Foundation between 2017 and 2019. He attended a scientific advisory board meeting of the Novo Nordisk Foundation Center for Basic Metabolic Research, University of Copenhagen, in 2016. He received funding for his research projects by Novo Nordisk (2016–2020) and Sanofi-Aventis (2012–2019). He was a consultant for Bionorica SE (2013–2017), Menarini Ricerche (2016), and Bayer Pharma AG Berlin (2016). As former Director of the Helmholtz Diabetes Center and the Institute for Diabetes and Obesity at Helmholtz Zentrum München (2011–2018) and since 2018, as CEO of Helmholtz Zentrum München, he has been responsible for collaborations with a multitude of companies and institutions, worldwide. In this capacity, he discussed potential projects with and has signed/signs contracts for his institute(s) and for the staff for research funding and/or collaborations with industry and academia, worldwide, including but not limited to pharmaceutical corporations such as Boehringer Ingelheim, Eli Lilly, Novo Nordisk, Medigene, Arbormed, BioSyngen and others. In this role, he was/is responsible for commercial technology transfer activities of his institute(s), including diabetes-related patent portfolios of Helmholtz Zentrum München (for example, WO/2016/188932 A2 or WO/2017/194499 A1). M.H.T. confirms that to the best of his knowledge none of the above funding sources was involved in the preparation of this paper. T.D.M. receives research funding from Novo Nordisk and has received speaking fees from Eli Lilly, AstraZeneca and Novo Nordisk. RDDiM is a co-inventor on intellectual property owned by Indiana University and licensed to Novo Nordisk. He was previously employed by Novo Nordisk. Y.H., P.J.K., B.Y., W.F.J.H., B.F. and J.D.D. are current employees of Novo Nordisk. The remaining authors declare no competing interests.

Additional information

Extended data is available for this paper at https://doi.org/10.1038/s42255-023-00931-7.

Supplementary information The online version contains supplementary material available at https://doi.org/10.1038/s42255-023-00931-7.

Correspondence and requests for materials should be addressed to Timo D. Müller.

Peer review information *Nature Metabolism* thanks Tune Pers, Alice Adriaenssens and the other, anonymous, reviewer for their contribution to the peer review of this work. Primary Handling Editor: Christoph Schmitt, in collaboration with the *Nature Metabolism* team.

https://doi.org/10.1038/s42255-023-00931-7

[1]Institute for Diabetes and Obesity, Helmholtz Diabetes Center, Helmholtz Munich, Neuherberg, Germany. [2]German Center for Diabetes Research (DZD), Neuherberg, Germany. [3]Department of Physiology, Faculty of Medical Sciences in Katowice, Medical University of Silesia, Katowice, Poland. [4]Institute of Physiotherapy and Health Sciences, Academy of Physical Education, Katowice, Poland. [5]Institute of Diabetes and Regeneration Research, Helmholtz Diabetes Center, Helmholtz Zentrum München, Neuherberg, Germany. [6]TUM School of Medicine, Technical University of Munich, Munich, Germany. [7]Core Facility Pathology & Tissue Analytics, Helmholtz Munich, Neuherberg, Germany. [8]Novo Nordisk Research Center Indianapolis, Indianapolis, IN, USA. [9]Department of Medicine IV, University Hospital, LMU Munich, Munich, Germany. [10]Department of Chemistry, Indiana University, Bloomington, IN, USA. [11]Helmholtz Munich, Neuherberg, Germany. [12]Division of Metabolic Diseases, Department of Medicine, Technical University of Munich, Munich, Germany. ✉e-mail: timodirk.mueller@helmholtz-munich.de

https://doi.org/10.1038/s42255-023-00931-7

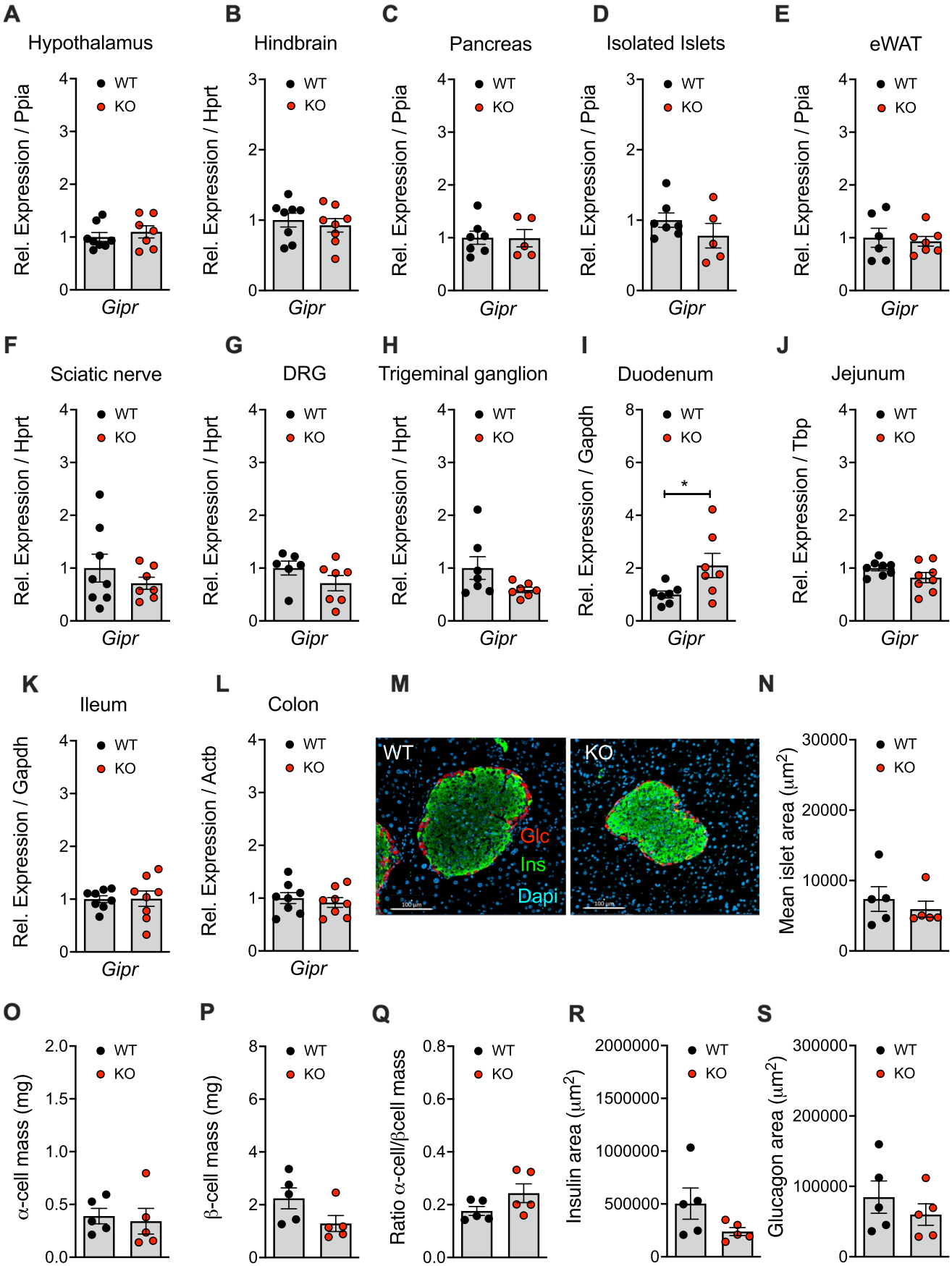

Extended Data Fig. 1 | See next page for caption.

https://doi.org/10.1038/s42255-023-00931-7

Extended Data Fig. 1 | Tissue-selective expression of *Gipr* in wild-type and *Vgat-Gipr* Ko mice. Expression of *Gipr* in hypothalamus (n = 7-8 each group) **(a)**, hindbrain (n = 8 each group) **(b)**, and pancreas (5-7 each group) of 40-wk old HFD-fed DIO male C57BL/6J wild-type and *Vgat-Gipr* KO mice **(c)**. Expression of *Gipr* in pancreatic islets isolated from 12-wk old male C57BL/6J wild-type and *Vgat-Gipr* KO mice **(d)** and Gipr expression in epididymal white adipose tissue (eWAT) (n = 6-7 each group) of 40-wk old HFD-fed DIO male C57BL/6J wild-type and *Vgat-Gipr* KO mice **(e)**. Expression of *Gipr* in sciatic nerve (n = 7-8 each group) **(f)**, dorsal root ganglia (DRG) (n = 6-7 each group) **(g)**, trigeminal ganglion (n = 7 each group) **(h)**, as well as in duodenum (n = 7 each group) **(i)**, jejunum (n = 8 each group) **(j)**, ileum (n = 8 each group) **(k)**, and colon (n = 8 each group) **(l)** of 12-wk old HFD-fed male C57BL/6J wild-type and *Vgat-Gipr* KO mice. Representative image of of insulin and glucagon immunostaining in pancreata of 38-wk old HFD-fed male C57BL/6J wild-type and *Vgat-Gipr* KO mice (n = 5 each group) **(m)**, and quantification of pancreatic islet area (n = 5 each group) **(n)**, α-cell mass (n = 5 each group) **(o)**, β-cell mass (n = 5 each group) **(p)**, α-cell/β-cell mass ratio (n = 5 each group) **(q)**, as well insulin area (n = 5 each group) **(r)** and glucagon area (n = 5 each group) **(s)** in 38-wk old male HFD-fed C57BL/6J wild-type and *Vgat-Gipr* KO mice. Data were analyzed using student's 2-sided, two-tailed t-test. Data represent mean ± SEM. Asterisk indicates * $p < 0.05$. Individual p values are shown in the Data Source file.

https://doi.org/10.1038/s42255-023-00931-7

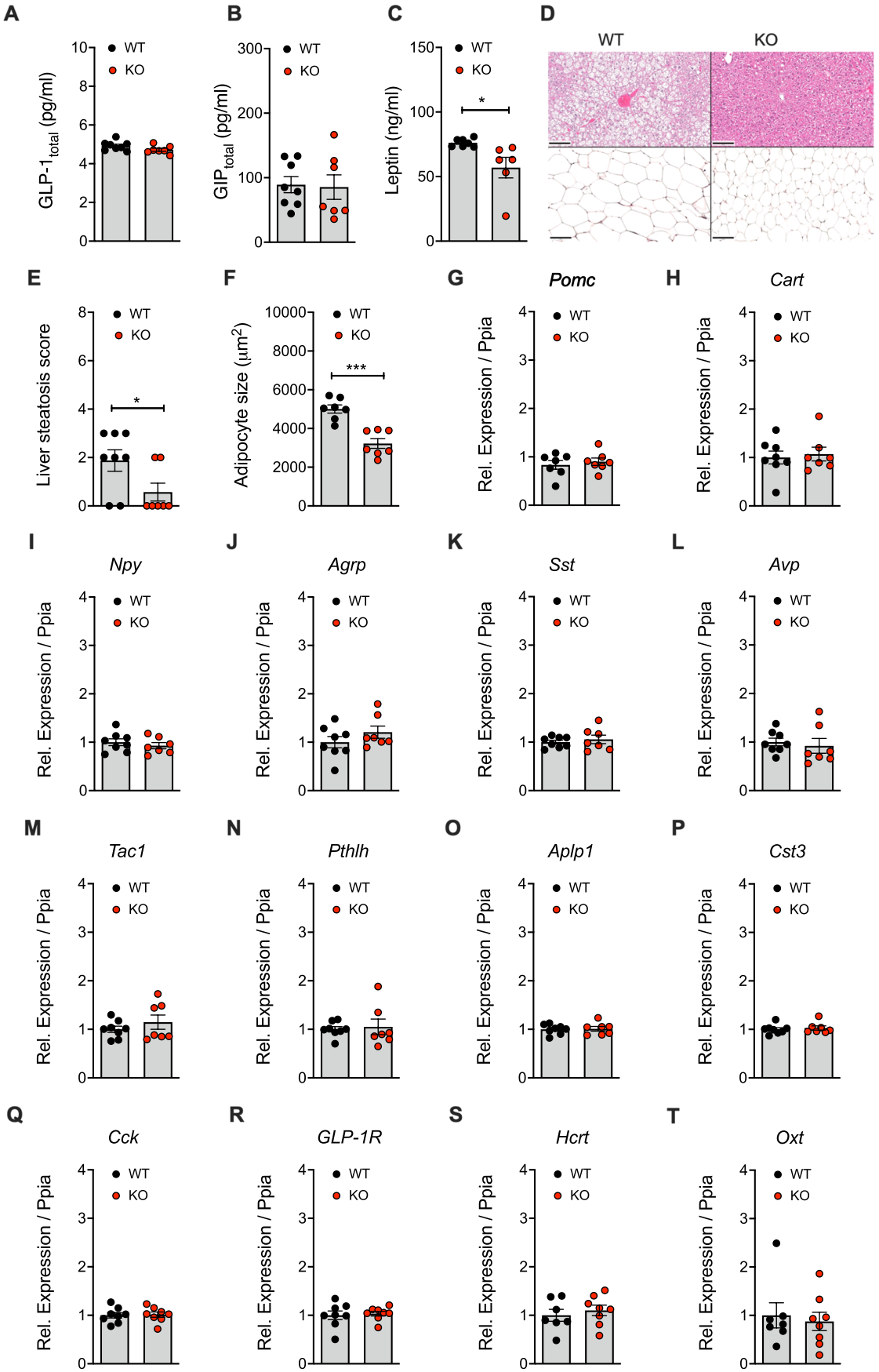

Extended Data Fig. 2 | See next page for caption.

https://doi.org/10.1038/s42255-023-00931-7

Extended Data Fig. 2 | Tissue histology and hypothalamic target gene expression in DIO wild-type and *Vgat-Gipr* KO mice. Ad libitum plasma levels of GLP-1_{total} **(a)** and GIP_{total} **(b)** in 40-wk old male C57BL/6J DIO wild-type and Vgat-Gipr KO mice mice (n = 7-8 each group). Serum levels of leptin in 40-wk old male C57BL/6J DIO wild-type and Vgat-Gipr KO mice (n = 6-7 each group) **(c)**, representative H&E staining of liver and inguinal white adipose tissue (iWAT) in 40-wk old C57BL/6J mice (n = 7-8 each group, scale bar: 100µm) **(d)**, corresponding steatosis score (n = 7-8 each group) **(e)** and mean iWAT adipocyte size (n = 7 each group) **(f)**, as well as hypothalamic expression of proopiomelanocortin; *Pomc* (n = 7 each group) **(g)**, cocaine and amphetamine regulated transcript; *Cart* (n = 7-8 each group) **(h)**, neuropeptide y; *Npy* (n = 7 each group) **(i)**, agouti-related peptide; *Agrp* (n = 7 each group) **(j)**, somatostatin; *Sst* (n = 7 each group) **(k)**, arginine vasopressin; *Avp* (n = 7 each group) **(l)**, tachykinin precursor 1; *Tac1* (n = 7 each group) **(m)**, parathyroid hormone like hormone; *Pthlh* (n = 7 each group) **(n)**, amyloid beta precursor like protein 1; *Aplp1* (n = 7 each group) **(o)** and cystacin c; *Cst3* (n = 7 each group) **(p)** in 40-wk old male C57BL/6J DIO wild-type and *Vgat-Gipr* KO mice. Expression of cholescystokinin; *Cck* **(q)**, *GLP-1R* **(r)**, hypocretin neuropeptide precursor; *Hcrt* **(s)** and oxytocin; *Oxt* **(t)** in the hindbrain of 40-wk old male C57BL/6J DIO wild-type and *Vgat-Gipr* KO mice. Data were analyzed using student's 2-sided, two-tailed t-test. Date represent mean ± SEM. Asterisks indicate * $p < 0.05$; ** $p < 0.01$ and *** $p < 0.001$. Individual p values are shown in the Data Source file.

https://doi.org/10.1038/s42255-023-00931-7

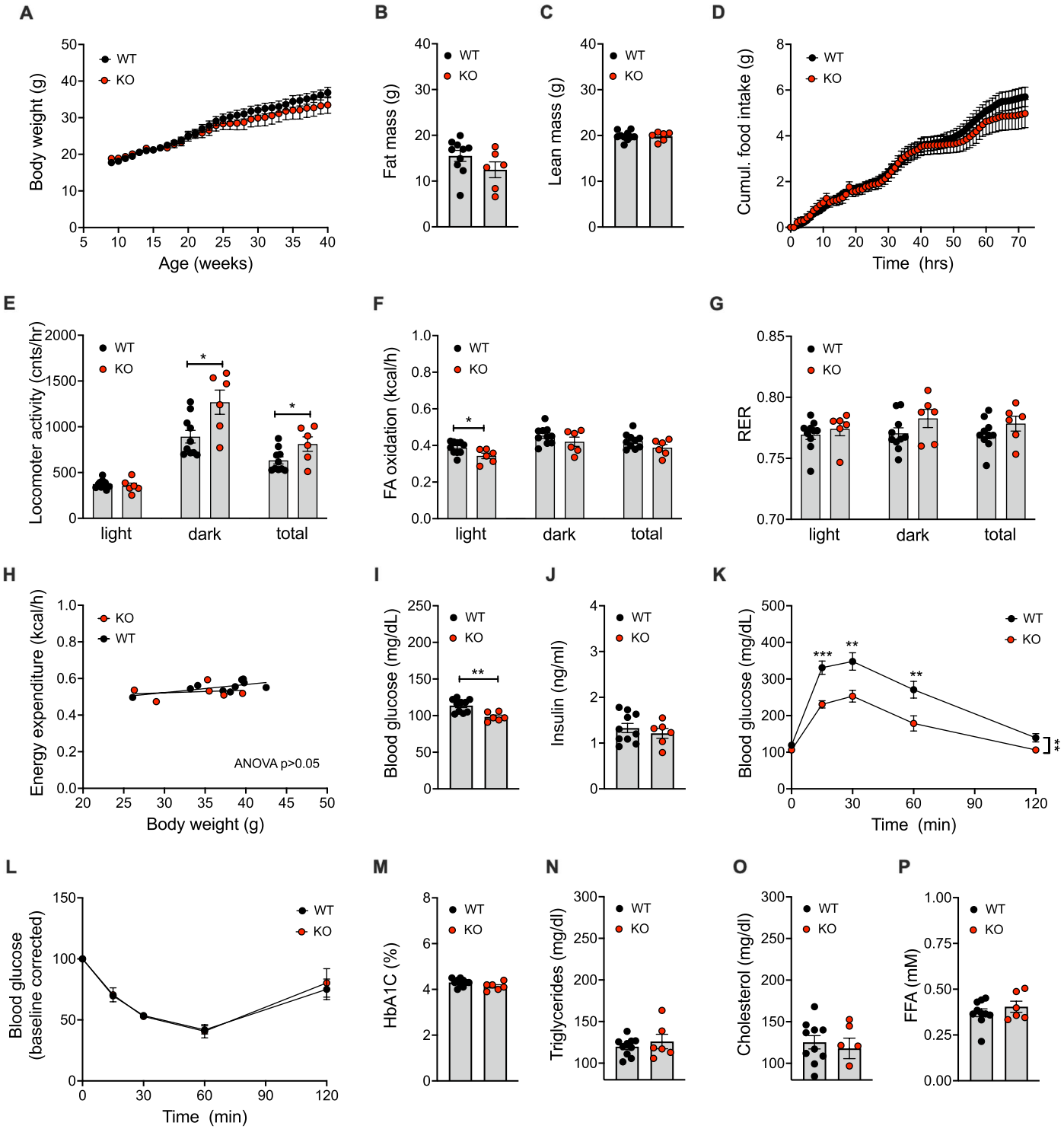

Extended Data Fig. 3 | Metabolic characterization of female HFD-fed *Vgat-Gipr* KO mice. Body weight development **(a)**, and body composition **(b)** of 40-wk old female HFD-fed C57BL/6J wild-type (WT) and *Vgat-Gipr* KO (KO) mice (WT/KO n = 10/6 mice). Cumulative food intake **(d)**, as well as locomotor activity **(e)**, fatty acid (FA) oxidation **(f)**, respiratory exchange ratio (RER) **(G)** and energy expenditure **(h)** in 40-wk old female C57BL/6J mice (WT/KO n = 10/6 mice). Fasting plasma levels of blood glucose **(i)** and insulin **(j)** in 43-wk old female C57BL/6J mice (WT/KO n = 10/6 mice), intraperitoneal glucose tolerance in 42-wk old female C57BL/6J mice (WT/KO n = 10/6 mice) **(k)**, intraperitoneal insulin tolerance in 42-wk old female C57BL/6J mice (WT/KO n = 9/6 mice) **(l)** and plasma levels HbA1c **(m)**, triglycerides **(n)**, cholesterol **(o)** and free fatty acids **(p)** in 44-wk old female C57BL/6J mice (WT/KO n = 10/6 mice). Data in panel **A,D,K and L** were analyzed by repeated measures 2-way ANOVA with Bonferroni's post hoc test for comparison of individual time points. Data in panel **B,C,E-G,I,J,M-P** were analyzed using student's 2-sided, two-tailed t-test. Data in panel **H** were analyzed using ANCOVA with body weight as covariate. Date represent means ± SEM; asterisks indicate * $p < 0.05$; ** $p < 0.01$ and *** $p < 0.001$. Individual p values are shown in the Data Source file.

https://doi.org/10.1038/s42255-023-00931-7

A

```
acyl-GIP    (IUB0271) YXEGT FISDY SIAMD KIHQQ DFVNW LLAQK GKKND WKHNI TQK (γE-γE-γE-C16)-OH
acyl-GLP-1  (IUB1746) HXEGT FTSDV SIYLD KQAAX EFVNW LLAGG PSSGA PPPSK(C16)
GLP-1/GIP   (MAR709)  YXEGT FTSDY SIYLD KQAAX EFVNW LLAGG PSSGA PPPSK(C16)
acyl-GIP^Cy5          YXEGT FISDY SIAXD KIRQQ KFVEW LLAQK E (Cy5)
acyl-GLP-1^Cy5        HXEGT FTSDV SSYLE EQAAK EFIAW LVKGG PSSGA PPPSK (Cy5)

X: Aminoisobutyric acid; Aib
X: Norleucine
K: Lysine(γE-OEG-OEG-C18)
```

Extended Data Fig. 4 | Sequence of the used GIP and GLP-1 analogs. Sequence of the used acyl-GIP, acyl-GLP-1, MAR709, acyl-GIP^{Cy5} and acyl-GLP-1^{Cy5} **(A)**.

https://doi.org/10.1038/s42255-023-00931-7

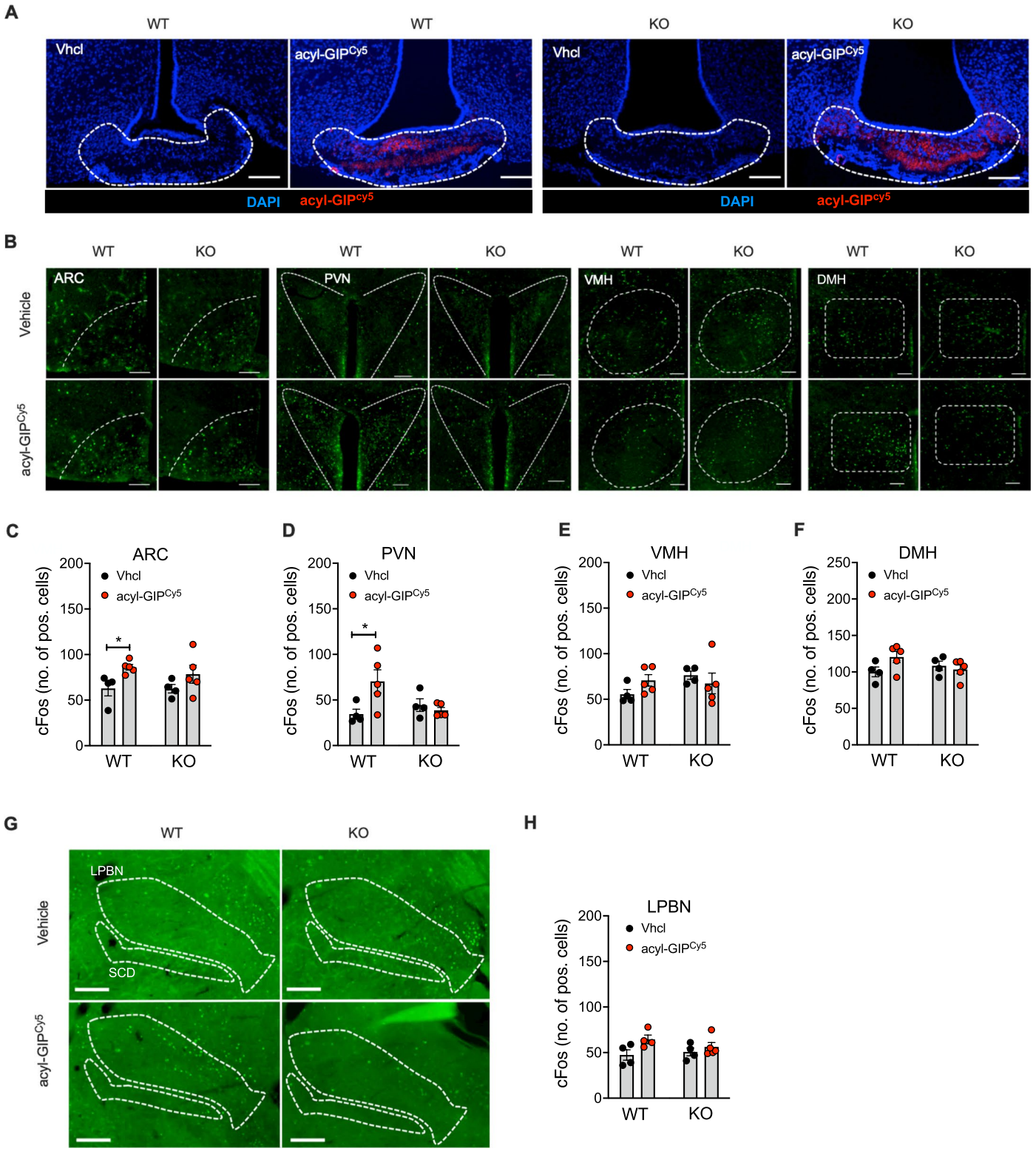

Extended Data Fig. 5 | Acyl-GIP effects on cFos neuronal activation in the hypothalamus in HFD-fed *Vgat-Gipr* KO mice. Representative image of hypothalamic acyl-GIP^{Cy5} fluorescence (n = 3-5 each group) **(a)** and cFos neuronal activity in the arcuate nucleus (ARC), paraventricular nucleus (PVN), ventromedial hypothalamus (VMH) and dorsomedial hypothalamus (DMH) (n = 4-5 each group) **(b)** in 26-wk old male C57BL/6J wild-type (WT) and *Vgat-Gipr* (KO) mice treated subcutaneous (s.c.) with a single dose of either vehicle or acyl-GIP^{Cy5} (150 nmol/kg; n = 3-5 each group). Corresponding cFos quantification in the ARC (n = 4-5 each group) **(c)**, PVN (n = 4-5 each group) **(d)**, VMH (n = 4-5 each group) **(e)**, and DMH (n = 4-5 each group) **(f)**. CFos neuronal activity (G) and corresponding cFos quantification (H) in the lateral parabrachial nucleus (LPBN) in 26-wk old male C57BL/6J WT and *Vgat-Gipr* (KO) mice treated s.c. with a single dose of either vehicle or acyl-GIP^{Cy5} (150 nmol/kg; n = 4-5 each group). Data in panel **C-F,H** were analyzed using student's 2-sided, 2-sided, 2-tailed t-test. Scale bars in panels **A** and **B** are 100 µm, scale bars in panel **G** are 200 µm. Data represent means ± SEM; asterisks indicate * $p < 0.05$. Individual p values are shown in the Data Source file.

https://doi.org/10.1038/s42255-023-00931-7

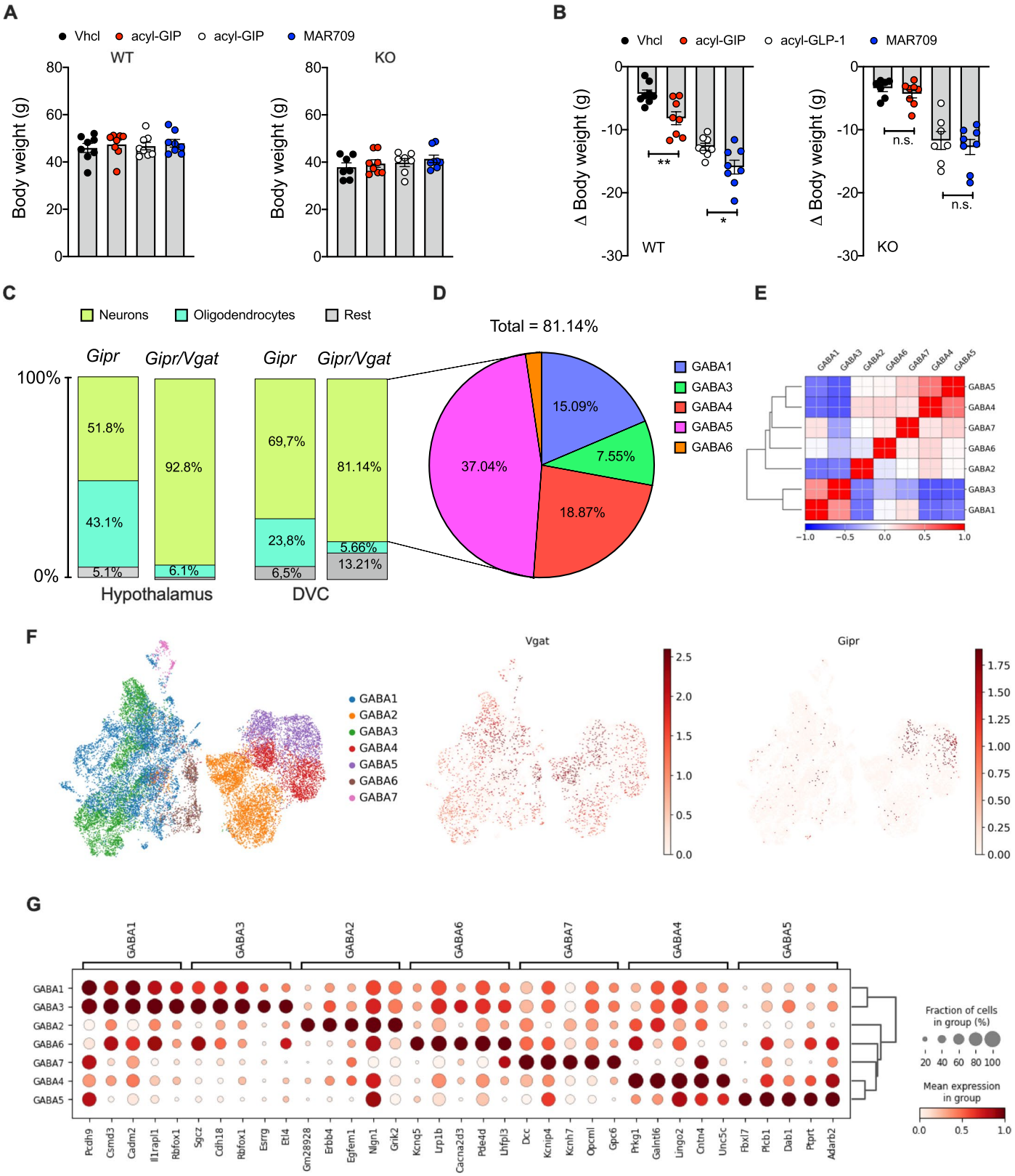

Extended Data Fig. 6 | See next page for caption.

https://doi.org/10.1038/s42255-023-00931-7

Extended Data Fig. 6 | Effects of acyl-GIP, acyl-GLP-1 and MAR709 on absolute body weight in HFD-fed *Vgat-Gipr* KO mice, and analysis of *Vgat/Gipr* in published scRNA repositories. Starting body weight **(a)** and body weight change **(b)** in 38-wk old male C57BL/6J wild-type (WT) or *Vgat-Gipr* KO mice treated daily with either Vehicle, acyl-GIP (100 nmolkg), or 10 nmol/kg of either acyl-GLP-1 or MAR709 (n = 7-8 each group). Cell types expressing *Vgat* and/or *Gipr* in the hypothalamus and dorsal vagal complex (DVC) **(c)**. Distribution of cells co-expressing *Gipr* and *Vgat* within 7 clusters of GABAergic neurons identified in the DVC **(d)**. Correlation plots with Pearson's correlations between 7 clusters (GABA1-7) of GABAergic neurons in the DVC **(e)**. UMAP of GABAergic neurons in the DVC colored by GABAergic neuron cluster, and expression of Vgat and Gipr in each cell, with the color corresponding to log-normalized UMI counts scaled to the maximum of each gene **(f)**. The dot plot of the top 5 genes most associated with each GABAergic neuron population as determined by Wilcoxon-rank-sum test **(g)**. Data in panel **A** were analyzed using ordinary 1-way ANOVA, data in panel **B** were analyzed using ordinary 1-way ANOVA and using Holm-Sidak multiple comparison test. Date represent means ± SEM; asterisks indicate * $p < 0.05$; ** $p < 0.01$ and *** $p < 0.001$. Individual p values are shown in the Data Source file, unless $p < 0.0001$. Data shown in panels C, D, E, F, G were generated based on publicly available snRNA Seq datasets of hypothalamus (Steuernagel et al.[15]) or DVC (Lugwig et al.[17]).

https://doi.org/10.1038/s42255-023-00931-7

Extended Data Table 1 | Overview of hypothalamic and hindbrain Gipr and Vgat expression based on published murine scRNA-seq studies

		Total Cells	Gipr cells		*Vgat* cells		*Gipr/Vgat* cells		*Gipr/Vgat* cells	*Gipr/Vgat* cells	Ref.
	Cluster	(no.)	(no.)	(%)	(no.)	(%)	(no.)	(%)	(% of Gipr cells)	(% of Gipr/Vgat cells)	
Hypothalamus	Astrocytes	52,186	15	0.03	2,166	4.15	1	0.00	6.67	0.27	Ref.15
	Endothelial cells	1,0261	26	0.25	269	2.62	2	0.02	7.69	0.53	
	Ependymal cells	4,425	11	0.25	198	4.47	0	0.00	0.00	0.00	
	Erythrocytes	41	0	0.00	3	7.32	0	0.00	0.00	0.00	
	Fibroblasts	41	5	0.36	68	4.96	0	0.00	0.00	0.00	
	Hypendymal cells	52	0	0.00	1	1.92	0	0.00	0.00	0.00	
	Microglial cells	14,304	6	0.04	716	5.01	1	0.01	16.67	0.27	
	Mural cells	3,776	24	0.64	218	5.77	0	0.00	0.00	0.00	
	Neurons	219,360	1,099	0.50	80,808	36.84	349	0.16	31.76	92.82	
	Oligodendrocytes	48,817	916	1.88	1,541	3.16	23	0.05	2.51	6.12	
	OPC	19,865	13	0.07	678	3.41	0	0.00	0.00	0.00	
	Pituitary gland cells	729	1	0.14	24	3.29	0	0.00	0.00	0.00	
	Tanycytes	9,737	7	0.07	340	3.49	0	0.00	0.00	0.00	
	Total	**384,925**	**2,123**	**0.55**	**87,030**	**22.61**	**376**	**0.10**	**17.7**	**100**	
Hindbrain (AP and NTS)	Neurons	9,179	208	2.27	1,950	21.24	52	0.57	25.00	88.14	Ref. 14
	Oligodendrocytes	5,463	222	4.06	151	2.76	7	0.13	3.15	11.86	
	OPC	582	5	0.86	20	3.44	0	0.00	0.00	0.00	
	Astrocytes	611	5	0.82	19	3.11	7	0.00	0.00	0.00	
	Microglia	392	5	1.28	9	2.30	0	0.00	0.00	0.00	
	Epithelial cells	133	5	3.76	4	3.01	0	0.00	0.00	0.00	
	Other	220	5	2.27	11	5.00	0	0.00	0.00	0.00	
	Total	**16,580**	**455**	**2.74**	**2,164**	**13.05**	**59**	**0.36**	**12.97**	**100**	
Hindbrain (AP only)	GABAergic Neurons	660	66	10.0	262	39.70	36	5.45	54.55	n/a	Ref. 21
	Glutamatergic Neurons	725	4	0.55	10	1.38	0	0.00	0.00	n/a	
	Total	**1,385**	**70**	**5.05**	**272**	**19.64**	**36**	**2.60**	**51.43**	**n/a**	
Hindbrain (DVC)	Astrocytes	9,419	17	0.18	205	2.18	0	0.00	0.00	0.00	Ref. 17
	Oligodendrocytes	6,481	176	2.72	156	2.41	3	0.05	1.70	5.66	
	OPC	1,770	4	0.23	47	2.66	0	0.00	0.00	0.00	
	Ependymal cells	1,737	9	0.52	46	2.65	1	0.06	11.11	1.89	
	Tanycyte-like cells	1,509	3	0.20	28	1.86	0	0.00	0.00	0.00	
	Endothelial cells	810	12	1.48	26	3.21	2	0.25	16.67	3.77	
	VLMCs	576	2	0.35	10	1.74	0	0.00	0.00	0.00	
	Microglia	434	1	0.23	16	3.69	0	0.00	0.00	0.00	
	All Glia Cells	22,736	224	0.98	534	2.35	6	0.03	2.68	11.32	
	GABA1	7,027	60	0.85	619	8.81	8	0.11	13.33	15.09	
	GABA2	4,167	15	0.36	462	11.09	0	0.00	0.00	0.00	
	GABA3	3,856	21	0.54	567	14.70	4	0.10	19.05	7.55	
	GABA4	2,359	54	2.29	223	9.45	10	0.42	18.52	18.87	
	GABA5	2,319	204	8.80	194	8.37	20	0.86	9.80	37.04	
	GABA6	978	4	0.41	136	13.91	1	0.10	25.00	1.89	
	GABA7	246	1	0.41	27	10.98	0	0.00	0.00	0.00	
	All GABAergic Neurons	20,952	359	1.71	2,228	10.63	43	0.21	11.98	81.13	
	All Glutamatergic Neurons	20,998	93	0.44	518	2.47	0	0.00	0.00	0.00	
	All Neurons	49,392	515	1.04	2,941	5.95	47	0.10	9.13	88.68	
	Total	**72,128**	**739**	**1.02**	**3,475**	**4.82**	**53**	**0.07**	**7.17**	**100.00**	

OPC: Oligodendrocyte precursor cells; AP: area postrema; NTS: nucleus tractus solitarius; DVC: dorsal vagal complex

nature portfolio

Corresponding author(s): Timo D. Müller

Last updated by author(s): Oct 9, 2023

Reporting Summary

Nature Portfolio wishes to improve the reproducibility of the work that we publish. This form provides structure for consistency and transparency in reporting. For further information on Nature Portfolio policies, see our Editorial Policies and the Editorial Policy Checklist.

Statistics

For all statistical analyses, confirm that the following items are present in the figure legend, table legend, main text, or Methods section.

n/a	Confirmed	
☐	☒	The exact sample size (*n*) for each experimental group/condition, given as a discrete number and unit of measurement
☐	☒	A statement on whether measurements were taken from distinct samples or whether the same sample was measured repeatedly
☐	☒	The statistical test(s) used AND whether they are one- or two-sided *Only common tests should be described solely by name; describe more complex techniques in the Methods section.*
☐	☒	A description of all covariates tested
☐	☒	A description of any assumptions or corrections, such as tests of normality and adjustment for multiple comparisons
☐	☒	A full description of the statistical parameters including central tendency (e.g. means) or other basic estimates (e.g. regression coefficient) AND variation (e.g. standard deviation) or associated estimates of uncertainty (e.g. confidence intervals)
☐	☒	For null hypothesis testing, the test statistic (e.g. *F*, *t*, *r*) with confidence intervals, effect sizes, degrees of freedom and *P* value noted *Give P values as exact values whenever suitable.*
☒	☐	For Bayesian analysis, information on the choice of priors and Markov chain Monte Carlo settings
☒	☐	For hierarchical and complex designs, identification of the appropriate level for tests and full reporting of outcomes
☐	☒	Estimates of effect sizes (e.g. Cohen's *d*, Pearson's *r*), indicating how they were calculated

Our web collection on statistics for biologists contains articles on many of the points above.

Software and code

Policy information about availability of computer code

Data collection	cFOS was imaged using LAS X (version 3.5.7.23225, Leica Microsystems CMS GmbH)
Data analysis	Statistical analyses were performed using GraphPad Prism version 9 and SPSS version 28.0.1.1. cFOS data were analyzed using QuPath (version 0.4.4). Single cell RNAseq analysis were analyzed using Scranpy (version 2.11.0), Seurat (v.5) or CellxGene (v. 1.1.2). Histological analysis were performed using Visiopharm (v. 2018.9)

For manuscripts utilizing custom algorithms or software that are central to the research but not yet described in published literature, software must be made available to editors and reviewers. We strongly encourage code deposition in a community repository (e.g. GitHub). See the Nature Portfolio guidelines for submitting code & software for further information.

Data

Policy information about availability of data

All manuscripts must include a data availability statement. This statement should provide the following information, where applicable:

- Accession codes, unique identifiers, or web links for publicly available datasets
- A description of any restrictions on data availability
- For clinical datasets or third party data, please ensure that the statement adheres to our policy

The data used for the statistical analysis are available in the data source file, along with the GraphPad Prizm-derived report on the statistical analysis as appropriate. The statistical report contains the mean difference between the treatment groups, the 95% confidence intervals, the significance summary, and the exact P values (unless P < 0.0001). The scRNAseq datasets used in the study are available via the GEO accession #GSE160938, #GSE166649 and #GSE168737. The used HypoMap is available in an interactive CellxGene viewer (https://www.mrl.ims.cam.ac.uk); the corresponding Seurat object is deposited at University of Cambridge's Apollo Repository (10.17863/CAM.87955). Other used databases include the Allen mouse atlas. All raw images are provided in the data source files, with exception of the

histology pictures for Extended Data Figures 1M-S and 2D-F, which were too large for public repositories. Due to the file size of these pictures, they are only available upon request.

Field-specific reporting

Please select the one below that is the best fit for your research. If you are not sure, read the appropriate sections before making your selection.

☒ Life sciences ☐ Behavioural & social sciences ☐ Ecological, evolutionary & environmental sciences

For a reference copy of the document with all sections, see nature.com/documents/nr-reporting-summary-flat.pdf

Life sciences study design

All studies must disclose on these points even when the disclosure is negative.

Sample size	For animal studies, sample sizes were calculated based on a power analysis assuming that a greater or equal (>/=) 5 g difference in body weight between genotypes can be assessed with a power of >/= 75% when using a 2-sided statistical test under the assumption of a standard deviation of 3.5 and an alpha level of 0.05.
Data exclusions	No data were excluded from the analysis unless scientific (e.g. significant outlier identified by the Grubbs test for outlier) or animal welfare reasons (e.g. injury due to fighting) demanded exclusion. Outliers are stated in the data source file.
Replication	In vivo and ex vivo data were obtained in independent biological replicates as indicated in the figure legends.
Randomization	Animals were either randomly assigned into treatment groups, or were grouped based on their genotype (WT or KO). At study start, only age-matched mice were included in the studies. There were no other covariats controlled.
Blinding	For in vivo studies, drugs were aliquoted by a lead scientist in number-coded vials and most, but not all, handling investigators were blinded to the treatment condition. Analyses of glucose and insulin tolerance were performed by experienced research assistants which did not know prior treatment conditions. Ex vivo studies were performed in ID coded vials without statement of treatment on the vials. Ex vivo studies were performed in ID coded vials, and with with most, but not all investigators, being blinded to the underlying genotypes.

Reporting for specific materials, systems and methods

We require information from authors about some types of materials, experimental systems and methods used in many studies. Here, indicate whether each material, system or method listed is relevant to your study. If you are not sure if a list item applies to your research, read the appropriate section before selecting a response.

Materials & experimental systems

n/a	Involved in the study
☐	☒ Antibodies
☒	☐ Eukaryotic cell lines
☒	☐ Palaeontology and archaeology
☐	☒ Animals and other organisms
☒	☐ Human research participants
☒	☐ Clinical data
☒	☐ Dual use research of concern

Methods

n/a	Involved in the study
☒	☐ ChIP-seq
☒	☐ Flow cytometry
☒	☐ MRI-based neuroimaging

Antibodies

Antibodies used	cFOS (Invitrogen, #MA5-15055; Dilution 1:400) anti-rabbit Alexa546 (Invitrogen, #A10040; Dilution1:2,000) anti-insulin (Cell Signaling, #3014, Dilution 1:800) AlexaFluor750-conjugated goat anti-rabbit (Invitrogen, A21039, Dilution 1:100) anti-glucagon (Takara, M182, Dilution 1:3000) goat anti-guinea pig AF555 (Invitrogen, A21435, Dilution 1:2000)
Validation	cFOS (Invitrogen, #MA5-15055): The cFOS monoclonal antibody Invitrogen #MA5-15055 was verified by Relative expression to ensure that the antibody binds to the antigen stated. The antibody shows reactivity in bovine, hamster, human, mouse, pig and rat. The antibody can be used for western blot, immunhistochemistry, immuncytochemistry, flow cytometry and ChIP assays. The antibody does not cross-react with other Fos proteins, including FosB, FRA1 and FRA2. Immunofluorescence analysis of c-Fos was performed using 70% confluent log phase HeLa cells treated with 200 ng/mL EGF for 30 min. The cells were fixed with 4% paraformaldehyde for 10 minutes, permeabilized with 0.1% Triton™ X-100 for 10 minutes, and blocked with 1% BSA for 1 hour at room temperature. The cells were labeled with c-Fos Monoclonal Antibody (T.142.5) (product # MA5-15055) at 1:250 dilution in 0.1% BSA, incubated overnight at 4 degree Celsius and then labeled with Goat anti-Rabbit IgG (H+L) Superclonal™

Anti-rabbit Alexa546 (Invitrogen, #A10040) is an Alexa Fluor 546-conjugated polyclonal donkey anti-rabbit antibody, supplied by Invitrogen Antibodies, cited in 648 publications, with 15 published images. Applications used include IHC, IHC-IF, ICC-IF, IF, and Others. These donkey anti-rabbit IgG (H+L) whole secondary antibodies have been affinity-purified and show minimum cross-reactivity to bovine, chicken, goat, guinea pig, hamster, horse, human, mouse, rat, and sheep serum proteins. Cross-adsorption or pre- adsorption is a purification step to increase specificity of the antibody resulting in higher sensitivity and less background staining. The secondary antibody solution is passed through a column matrix containing immobilized serum proteins from potentially cross-reactive species. Only the nonspecific-binding secondary antibodies are captured in the column, and the highly specific secondaries flow through. The benefits of this extra step are apparent in multiplexing/multicolor-staining experiments (e.g., flow cytometry) where there is potential cross-reactivity with other primary antibodies or in tissue/cell fluorescent staining experiments where there may be the presence of endogenous immunoglobulins. Alexa Fluor dyes are among the most trusted fluorescent dyes available today. InvitrogenTM Alexa Fluor 546 dye is a bright, orange-fluorescent dye with excitation ideally suited to the 546 nm laser line. For stable signal generation in imaging and flow cytometry, Alexa Fluor 546 dye is pH-insensitive over a wide molar range. Probes with high fluorescence quantum yield and highphotostability allow detection of low-abundance biological structures with great sensitivity. Alexa Fluor 546 dye molecules can be attached to proteins at high molar ratios without significant self-quenching, enabling brighter conjugates and more sensitive detection. The degree of labeling for each conjugate is typically 2-8 fluorophore molecules per IgG molecule; the exact degree of labeling is indicated on the certificate of analysis for each product lot.
Using conjugate solutions: Centrifuge the protein conjugate solution briefly in a microcentrifuge before use; add only the supernatant to the experiment. This step will help eliminate any protein aggregates that may have formed during storage, thereby reducing nonspecific background staining. Because staining protocols vary with application, the appropriate dilution of antibody should be determined empirically. For the fluorophore-labeled antibodies a final concentration of 1-10 µg/mL should be satisfactory for most immunohistochemistry and flow cytometry applications.

Insulin (C27C9) Rabbit mAb #3014 (Cell Signaling) is a validated monoclonal antibody used in 119 publications. Applications include Immunohistochemistry, ChIP, and Immunoprecipitation. The antibody reacts with Insulin from human, mouse and rat. Based on the manufacturer, the antibody meats all of the quality control standards defined by Cell Signaling Technology, Inc. Validations include Immunohistochemical analysis of paraffin-embedded human pancreas, showing the staining of β cells, using Insulin (C27C9) Rabbit mAb. The antibody is further reported to show very clear staining at 1:2000 with no background staining in primary human cells

AlexaFluor750-conjugated goat anti-rabbit (Invitrogen, A21039). An Alexa Fluor 750-conjugated polyclonal goat anti-rabbit antibody, supplied by Invitrogen Antibodies, cited in 72 publications, with 1 published image. Applications used include WB, IHC, IHC-IF, FC/FACS, and 3 Others.

anti-glucagon (Takara, M182) is a polyclonal guinea pig antibody, supplied by Takara Bio, cited in 24 publications. Applications used include IHC and CLARITY. Its a Guinea Pig polyclonal antibody raised against the peptide [HSQGTFTSDYSKYLDSRRAQDFVQWLMNT] of human Glucagon conjugated with KLH as an immunogen.The lyophilized antibody was dissolved in 50 µl of specifed water. The antibody dilutions were applied for ELISA assay by colorimetric detection using a microtiter plate immobilized with human Glucagon peptide. The expected antibody titration was obtained. Manufacturing Control:
Purification: Guinea Pig serum IgG was purified by affinity column chromatography, dissolved in 10 mM PBS, pH 7.4, containing 1.0% bovine serum albumin, and then lyophilized. The lyophilized antibody does not contain preservative.

goat anti-guinea pig AF555 (Invitrogen, A21435) is an Alexa Fluor 555-conjugated polyclonal goat anti-guinea pig antibody, supplied by Invitrogen Antibodies, cited in 215 publications, with 1 published image. Applications used include IHC, IHC-IF, ICC, ICC-IF, and 9 Others.

Animals and other organisms

Policy information about studies involving animals; ARRIVE guidelines recommended for reporting animal research

Laboratory animals

Figure 1A-J: 35-wk old male C57BL/6J Vgat Cre+/- Gipr wt/wt (WT) and Vgat Cre+/- Gipr flx/flx (KO) mice
Figure 1K and L: 37-wk old male C57BL/6J Vgat Cre+/- Gipr wt/wt (WT) and Vgat Cre+/- Gipr flx/flx (KO) mice
Figure 1M and N: 38-wk old male C57BL/6J Vgat Cre+/- Gipr wt/wt (WT) and Vgat Cre+/- Gipr flx/flx (KO) mice
Figure 1O and P: 34-wk old male C57BL/6J wVgat Cre+/- Gipr wt/wt (WT) and Vgat Cre+/- Gipr flx/flx (KO) mice
Figure 1Q-T: 40-wk old male C57BL/6J Vgat Cre+/- Gipr wt/wt (WT) and Vgat Cre+/- Gipr flx/flx (KO) mice
Figure 2A-J: 36-wk old male C57BL/6J Vgat Cre+/- Gipr wt/wt (WT) and Vgat Cre+/- Gipr flx/flx (KO) mice
Figure 2K-M: 38-wk old male C57BL/6J Vgat Cre+/- Gipr wt/wt (WT) and Vgat Cre+/- Gipr flx/flx (KO) mice
Figure 2N: 39-wk old male C57BL/6J Vgat Cre+/- Gipr wt/wt (WT) and Vgat Cre+/- Gipr flx/flx (KO) mice
Figure 2O and P: 40-wk old male C57BL/6J Vgat Cre+/- Gipr wt/wt (WT) and Vgat Cre+/- Gipr flx/flx (KO) mice
Figure 3A-C: 52-wk old male C57BL/6J wildtype mice
Figure 3D and E: 26-wk old male C57BL/6J Vgat Cre+/- Gipr wt/wt (WT) and Vgat Cre+/- Gipr flx/flx (KO) mice
Figure 3F and G: 35-wk old male C57BL/6J Vgat Cre+/- Gipr wt/wt (WT) and Vgat Cre+/- Gipr flx/flx (KO) mice
Figure 3H and I: 40-wk old female C57BL/6J Vgat Cre+/- Gipr wt/wt (WT) and Vgat Cre+/- Gipr flx/flx (KO) mice
Figure 4A-I: 38-wk old male C57BL/6J Vgat Cre+/- Gipr wt/wt (WT) mice
Figure 4J: 35-wk old male C57BL/6J Vgat Cre+/- Gipr wt/wt (WT) mice
Figure 4K-T: 35-wk old male C57BL/6J Vgat Cre+/- Gipr flx/flx (KO) mice
Extended Data Figure 1 A-C, E: 40-wk old male C57BL/6J Vgat Cre+/- Gipr wt/wt (WT) and Vgat Cre+/- Gipr flx/flx (KO) mice
Extended Data Figure 1 D, x-wk old male C57BL/6J Vgat Cre+/- Gipr wt/wt (WT) and Vgat Cre+/- Gipr flx/flx (KO) mice
Extended Data Figure 1 F-S: 38-wk old male C57BL/6J Vgat Cre+/- Gipr wt/wt (WT) and Vgat Cre+/- Gipr flx/flx (KO) mice
Extended Data Figure 2 A-T: 40-wk old male C57BL/6J Vgat Cre+/- Gipr wt/wt (WT) and Vgat Cre+/- Gipr flx/flx (KO) mice
Extended Data Figure 3A-H: 40-wk old female Vgat Cre+/- Gipr wt/wt (WT) and Vgat Cre+/- Gipr flx/flx (KO) mice
Extended Data Figure 3I,J: 43-wk old female Vgat Cre+/- Gipr wt/wt (WT) and Vgat Cre+/- Gipr flx/flx (KO) mice
Extended Data Figure 3K: 42-wk old female Vgat Cre+/- Gipr wt/wt (WT) and Vgat Cre+/- Gipr flx/flx (KO) mice
Extended Data Figure 3L-P: 44-wk old female Vgat Cre+/- Gipr wt/wt (WT) and Vgat Cre+/- Gipr flx/flx (KO) mice
Extended Data Figure 5: A-F, 26-wk old male C57BL/6J Vgat Cre+/- Gipr wt/wt (WT) and Vgat Cre+/- Gipr flx/flx (KO) mice
Extended Data Figure 6: A,B, E: 38-wk old male C57BL/6J Vgat Cre+/- Gipr wt/wt (WT) and Vgat Cre+/- Gipr flx/flx (KO) mice

Wild animals	no wild animals were used in the study
Field-collected samples	no field collected animals were used in the study
Ethics oversight	Experiments were performed in accordance with the Animal Protection Law of the European Union after permission by the Government of Upper Bavaria, Germany

Note that full information on the approval of the study protocol must also be provided in the manuscript.